KEK Proceedings 2002-26
March 2003
A

Proceedings of the Mini-Workshop on *Channeling Radiation Phenomena and Positron Production*

17 January, 2003, KEK, Tsukuba

Editors

Tsuyoshi Suwada and Masanori Satoh

KEK, High Energy Accelerator Research Organization,
Oho 1-1, Tsukuba, Ibaraki, 305-0801 Japan

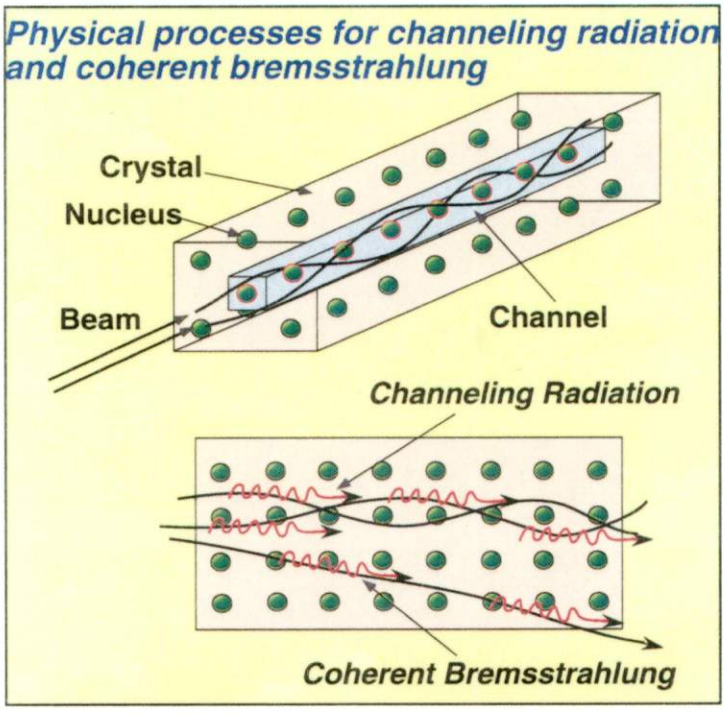

High Energy Accelerator Research Organization

Memorandum on mini-workshop "Positron production in oriented crystals"

V. N. Baier
Budker Institute of Nuclear Physics,
Novosibirsk, 630090, Russia

January 22, 2003

During last two years the results were published for the first time of quantitative study of positron production from high energy electrons in oriented single crystals. The rate of positron yield was measured in tungsten, silicon and diamond axially oriented crystals with accuracy of order $15 \div 20\%$. The obtained data are in quite satisfactory agreement with the theory and based on this theory simulation. This may be considered as a summary of reports presented at mini-workshop.

In my opinion this means that now is just a time to make the next step and start investigation of optimization of the positron source. This includes:

1. Reasonable definition of needed intensity of positron source. What is the optimal energy both for electron and positron? For KEKB factory the current requirements are known.

2. For Japan Linear Collider project one can start from existing project.

3. Transverse size and angular width of beams? For positions these beam characteristics are defined basically by the source matching system.

4. Search of optimal crystal type, its thickness, distance between crystal and amorphous parts (for combined target) taking into account energy losses both in the crystal and target. What are maximal permitted energy losses, their dependence on the beam size?

5. Calculation and measurement of positron yield. One can expect that increase of positron yield in crystal comparing with amorphous target will be of the order $1.3 \div 1.5$ and diminishing of energy losses in crystal comparing with amorphous target will be at least 2 times.

A lot of efforts are needed to solve these problems. It seems promising if this investigation will be done by an international collaboration including KEK, Tokyo MU, BINP(Novosibirsk), ...

Positron production in axially oriented single crystals: comparison of theory with experiment

V. N. Baier and V.M. Strakhovenko
Budker Institute of Nuclear Physics,
Novosibirsk, 630090, Russia

February 20, 2003

Abstract

The theory of radiation from high energy electrons moving near a crystalline axis is outlined. The intensity of radiation in thick crystal is discussed. Starting from the energy $\varepsilon \sim 1$ GeV the contribution of channeling radiation dominates. For energies a few GeV the development of the electron - photon showers in axially aligned single crystals is described including the formula for the intensity spectrum. Both channeling radiation and bremsstrahlung are taken into account. Some characteristics of the positron yield measured in recent experiments are calculated. Theoretical estimations display a rather good agreement with experimental results obtained using 3 to 10 GeV electrons aligned to the $< 111 >$ - axis of the tungsten crystals. Such comparison verified that the accuracy of our approach is quite sufficient to make a reliable choice for optimal parameters of the positron source using axially aligned crystals for future linear colliders.

1 Introduction

An efficient positron source is one of the important components of future electron - positron colliders. Positrons are generated from electrons in the course of the $e^-e^+\gamma$ - shower developing in a medium. In high-energy region, the basic processes involved in the shower development are typically considerably enhanced in oriented crystals as compared with corresponding amorphous media . The most pronounced effects take place at axial alignment when initial electrons are moving along the main axes of a crystal. This alignment alone will be considered below.

1.1 Radiation in axially oriented crystals

A theoretical description of the specific radiation which occurs when high-energy particles are moving near the crystalline axes in single crystals depends essentially on whether a crystal is thin or thick. In thin crystal, by definition, the distribution

function (DF) in a transverse (to the direction of the axes) phase space doesn't vary when a particle passes through a crystal and is defined by the initial conditions. In thick crystals, a dependence of the DF on the depth of penetration of particles into a crystal should be taken into account. A multiple scattering and radiation energy losses are the basic processes which govern the kinetics of the DF.

The effect under discussion can be used as a source of hard and directed radiation concentrated within a comparatively narrow frequency range [1]. Thick crystals are of greatest interest for applications of the mentioned specific radiation in the range of not too high energies. One of the most important characteristics is the total radiation intensity into a given solid angle. Different properties of radiation in thick axially oriented crystals were analyzed in [1], [2], [3], [4].

According to the analysis performed in [4] where the kinetics was due to multiple scattering, the DF for large depth l is of the form

$$dF(\mathbf{v}_\perp, \boldsymbol{\varrho}, l) = \frac{d^2\varrho}{S}\frac{d^2v_\perp}{\pi g(l)}\exp\left(-\frac{v_\perp^2}{g(l)}\right), \tag{1.1}$$

where $\boldsymbol{\varrho} = \boldsymbol{\varrho}(x, y)$ are the transverse coordinates, $|\boldsymbol{\varrho}| \leq r_0$, $S = \pi r_0^2$ is the area of a cell in the transverse plane which contains the projection of one atomic chain, and $n_\perp = 1/S$ is the density of chains of atoms (axes). The function $g(l)$ has the form

$$g(l) = \Delta^2 + \int_0^l \dot{\vartheta}_s^2(t)dt, \tag{1.2}$$

where $\dot{\vartheta}_s^2$ is the rate of variation of the squared angle of multiple scattering in an appropriate amorphous medium. The time (depth) dependence of $\dot{\vartheta}_s^2$ is connected with the variation of the particle energy because of radiation losses.The first term in $g(l)$ reflects the character of the angular (over the transverse velocity) distribution established at the initial stage of electron motion in a crystal which depends on the angular (over the angle of incidence ϑ_0) distribution in an incident beam. Even in the case $\vartheta_0 = 0$, the angular spread of particles in the crystal proves to be roughly equal to the Lindhard angle, $\vartheta_c = \sqrt{2U_0/\varepsilon}$ (U_0 is the depth of the potential well of the axis, ε is the energy of a particle). Therefore, assuming the incident beam to be rather narrow, $\vartheta_0 \leq \vartheta_c$, we put in [1] $\Delta^2 = \vartheta_c^2$.

In thick crystals some processes, mainly, multiple scattering and radiation energy losses change the DF. The multiple scattering, on the average, increases particle transverse energy. As a result, particles can leave a channel(dechanneling). We introduce the critical dechanneling length owing to multiple scattering l_d over which the root mean square angle of scattering becomes equal to the Lindhard angle ϑ_c:

$$l_d = \frac{\alpha}{4\pi}\left(\frac{\varepsilon\vartheta_c}{m}\right)^2 L_{rad}, \tag{1.3}$$

where m is the electron mass, and L_{rad} is the radiation length in an appropriate amorphous medium.

For energies from several hundreds of MeV to several GeV and crystal thickness $L \gg l_d$ we have for the multiple scattering angle $\vartheta_s \gg 1/\gamma$ and $\vartheta_s \gg \vartheta_c$, then

the factor $\exp\left(-\frac{v_\perp^2}{g(l)}\right)$ can be substituted for unity and the distribution proves to be uniform in a transverse phase space. As a consequence, for the intensity of the radiation under consideration (labeled by ch) at the depth l we have

$$\frac{dI_{ch}}{d\Omega} = \frac{\bar{I}}{\pi g(l)}, \tag{1.4}$$

where $\bar{I} = \int I(\varrho) d^2\varrho / S$. It is worth to note that $\bar{I}$ coincides with I_{as}, the asymptotic value achieved by the radiation intensity at the angle of incidence $\vartheta_0 \geq \vartheta_c$. One should emphasize that Eq.(1.4) incorporates the radiation from channeled particles as well as from the above-barrier ones. Appearance of I_{as} in Eq.(1.4) is due to the uniformity of the distribution in the transverse phase space under indicated assumptions, while the uniformity of the distribution with respect to $v_\perp$ resulted in Eq.(1.4) in a uniform distribution with respect to the solid angle of emitted photons for angles $\vartheta_{ph} \ll \vartheta_s$.

The values of $\bar{I} = I_{as}$ can be readily calculated for any potential of the axes. We use the axial potential in the form (see [2], [3])

$$U(x) = V_0 \left[\ln\left(1 + \frac{1}{x+\eta}\right) - \ln\left(1 + \frac{1}{x_0+\eta}\right) \right]. \tag{1.5}$$

Neglecting recoil effects (or, in other words, using the classical theory) we obtain for this potential

$$\bar{I} = I_{as} = I_0 \varphi(\eta), \tag{1.6}$$

where

$$I_0 = \frac{8\pi e^2 V_0^2 \varepsilon^2}{3m^4} n_\perp, \quad \varphi(\eta) = (1+2\eta)\ln\left(1+\frac{1}{\eta}\right) - 2. \tag{1.7}$$

In Eq.(1.5) $x = \varrho^2/a_s^2$, a_s is the screening radius, $x_0 = r_0^2/a_s^2$, and the parameter η is proportional to the squared amplitude of thermal vibrations u_1. The fitting parameters V_0, a_s, η are given in Table 1 for the $< 111 >$ axis.

A simple estimation of the range of typical photon energies being radiated is evidently useful. The characteristic radius of the region giving the main contribution to the radiation is the screening radius a_s (see also [2], [3]). The transverse velocity of the electron in the channel is $v_\perp \leq \vartheta_c$. Therefore, the corresponding frequency of motion is ϑ_c/a_s and the corresponding radiation frequency, with the Doppler effect taken into account, is equal to

$$\omega_{ch} \simeq 2\gamma^2 \frac{\vartheta_c}{a_s} \tag{1.8}$$

This estimate is valid in the dipole case, when the corresponding parameter

$$\rho = 2\gamma^2 \mathbf{v}_\perp^2, \tag{1.9}$$

where $\mathbf{v}_\perp$ is the transverse velocity of particle, is small ($\rho \ll 1$) and quantum recoil is neglected. In the case $\rho \gg 1$ the radiation is of magnetic bremsstrahlung type (that is higher harmonics dominate in the spectrum). So the parameter ρ characterizes the structure of radiation spectrum, it can be called the multipolar parameter.

For particle in the channel ($\vartheta_0 \leq \vartheta_c$) we have

$$\rho \simeq \rho_c = \frac{2V_0\varepsilon}{m^2}. \tag{1.10}$$

and at above-barrier motion ($\vartheta_0 \geq \vartheta_c$)

$$\rho \simeq \left(\frac{2V_0}{m\vartheta_0}\right)^2 \tag{1.11}$$

The values of a_s, V_0 and other parameters for different crystals are given above in Table 1.

At high energies the quantum recoil becomes significant. The quantum character of radiation is determined by the parameter

$$\chi_s = \frac{eE_s\varepsilon}{m^3} = \frac{V_0\varepsilon}{a_s m^3}, \tag{1.12}$$

Where E_s is the typical value of the electric field of axis, $eE_s = V_0/a_s$. At $\chi_s \ll 1$ the classical theory is valid. Because of $\rho_c/\chi_s = 2a_s m \sim 10^2$ for crystals under consideration, at $\chi_s \sim 1$ where the radiation is essentially quantum, one has $\rho \sim 10^2$ so that radiation in this case is of the magnetic bremsstrahlung nature. However, one should take into account that the quantum effects in the magnetic bremsstrahlung are "turn on" rather early. For example, already at $\chi = 0.1$ the classical value of the total intensity of radiation is around 1.5 times larger than the correct value. Using quantum approach one finds [5] that quantum corrections exceed 10% at the energy near 5 GeV in Si and diamond and at the energy near 3 GeV in Ge. So, at the energy $\varepsilon = 1$ GeV the corrections to the numbers R given in Table 1 for mentioned crystals are small. The situation is different for tungsten where already at the energy of 1 GeV the correction to the radiation intensity is 23% at room temperature and 33% for T=77 K. This means that actually we have $R(1\text{ GeV}) = 1.14$ for tungsten at room temperature and $R(1\text{ GeV}) = 1.59$ at T=77 K.

Besides the radiation under study, the bremsstrahlung (below with the subscript "br") also contributes to the intensity. Actually, the bremsstrahlung process changes in comparison with an amorphous medium under channeling conditions [6]. Typical scale of this effect is of the order 10%. Therefore, for crude estimates one can use the bremsstrahlung intensity in a corresponding amorphous medium. Under assumptions used above, we have for the bremsstrahlung intensity at depth l

$$\frac{dI_{br}}{d\Omega} = \frac{I_{br}}{\pi g(l)} \equiv \frac{1}{\pi g(l)}\frac{\varepsilon}{L_{rad}}, \tag{1.13}$$

It follows from above analysis that radiation intensity in a crystal Si or Ge is of the order that of the conventional bremsstrahlung at electron energies $\varepsilon \simeq 1$ GeV. While in diamond and tungsten the radiation intensity exceeds that of the conventional bremsstrahlung at this energy. It is seen also that the spectrum of radiation is relatively soft. Basing on these properties of the photon emission process, the use of this phenomenon in positron source for future accelerators was proposed

Table 1: Parameters of the potential Eq.(1.5) for $< 111 >$ axis and some characteristics of the radiation

Crystal	u_1 (10^{-8}cm) T=293 K	V_0 (eV)	U_0 (eV)	η	a_s (10^{-8}cm)	R	ω_{ch} (MeV)	ρ_c
$C_{(d)}$	0.040	29	103	0.025	0.326	1.87	21.1	0.22
Si	0.075	54	106	0.150	0.30	0.80	23.3	0.41
Ge	0.085	91	191	0.13	0.30	0.53	31.1	0.7
W	0.050	417	937	0.115	0.215	1.48	31	3.2
W (77 K)	0.030	348	1255	0.027	0. 228	2.38	35	2.7

In the table u_1 is the amplitude of thermal vibrations, V_0, β, a_s are the parameters of the potential, U_0 is the depth of potential well, R=I_{as}/I_{br} ratio at $\varepsilon = 1$ GeV, ω_{ch} is the characteristic photon energy calculated by means Eq.(1.8), the parameter ρ_c Eq.(1.10) is calculated at $\varepsilon = 1$ Gev. For position of spectrum maximum in tungsten it is taken into account that at energy $\varepsilon = 1$ Gev radiation is nondipole ($\rho_c \simeq 3.2$)

[7]. The pair production rate which is due to the coherent (crystal) effects exceeds that of the standard (Bethe-Heitler) mechanism starting with photon energies $\omega \simeq \omega_{th}$. The value of ω_{th} is about 22 GeV for the $< 111 >$ - axis of tungsten being several times larger for another crystals. (See review [8] and recent book [9] for further details concerning QED - processes in crystals.) For energies well above ω_{th}, the crystal effects become really strong and may be used to create effective and compact electromagnetic calorimeters [10]. For very high energies ($\varepsilon \gg \omega_{th}$) of initial and created particles, kinetic equations describing the shower development were solved analytically [11]. Though the initial electron energies were high enough in the first experimental investigation [12] of shower formation in crystals, energies of detected particles were too low to allow us the direct comparison with [11]. To explain the results of [12], Monte-Carlo simulations were performed in [13]. The probabilities of basic processes used in [13] were obtained within so-called constant field approximation (CFA). A good agreement was demonstrated in [13] with the results of [12] for Ge crystals.

1.2 Electromagnetic showers in crystal at GeV energies [14]

When the initial electron energy is below ω_{th}, photons are mainly emitted with energies $\omega \ll \omega_{th}$ and so, up to minor modifications (see [17], [18]), the pair production process proceeds in a crystal as in an amorphous medium. The enhancement of radiation from initial electrons is thereby the main crystal effect in this energy region.

Here we consider the case when the angle of incidence ϑ_0 with respect to the chosen axis is not too large as compared to the Lindhard angle $\vartheta_c = (2U_0/\varepsilon)^{1/2}$, since in this case the most pronounced effects take place.

Let us start with the coherent contribution to the radiation. As already mentioned, at sufficiently high energies corresponding expressions valid at any ϑ_0 were obtained in [16]. For $\vartheta_0 \ll V_0/m$ they reproduce CFA-limit. But even if the initial electron energy is high enough to apply mentioned description, charged particles arising in the course of a shower development may not satisfy this condition. In the case of a soft cascade we have to describe the radiation from these "soft" particles as well. Let us remind that within semi-classical theory of the QED- processes in any external field there are only two parameters: ρ and χ. The parameter ρ is a measure of the particle velocity deviation from a straight line in units of the natural emission angle $\gamma^{-1} = m/\varepsilon$, while the parameter χ being the ratio of the external field strength in the particle rest system to the critical QED-value $E_c = 1.32 \cdot 10^{16}\, eV/cm$ is responsible for the magnitude of quantum recoil effects. Let us remind also that at $\rho \ll 1$ the dipole approximation for a description of the radiation is valid and a typical formation time is $\sim \omega_0^{-1}$, where ω_0 is the characteristic frequency of motion. At $\rho \gg 1$ CFA is valid, the radiation formation time is $\sim \omega_0^{-1}\rho^{-1/2}$, i.e. much less than a period of motion. In this case the description of the emission process becomes local and we do not need to know what the particle trajectory is like contrary to the case of small $\rho \leq 1$ when we have to know it . If we now recollect that generally the two-dimensional problem of particle motion has not been solved yet in an analytical form, then evidently the same is true for the much more complicated problem of obtaining a radiation spectrum at such motion. We emphasize that for the coherent contribution to the total intensity of radiation $I_{ch}(\varepsilon)$ CFA gives a correct result up to very small energies when semi-classical approximation is still valid (see corresponding discussion in [16]).

The known (see Eq.(1.4) in [16]) estimate for the characteristic frequency of emitted photons ω at given frequency of motion ω_0 reads

$$u \equiv \frac{\omega}{\varepsilon - \omega} \simeq \frac{2N\omega_0\varepsilon}{m^2\,(1 + \rho/2)}, \tag{1.14}$$

where N is the characteristic number of emitted harmonics. Note that N = 1 for $\rho \leq 1$ and N $\propto \rho^{3/2}$ for $\rho \gg 1$. Using also that $\omega_0 \sim \theta_0/a_s$, (see Eq.(1.8)) we suggest to describe the radiation from channeled and moving not very high above the potential barrier particles the following heuristic intensity spectrum:

$$\frac{dI_{ch}}{d\omega} = \frac{r(\varepsilon)\varepsilon}{u_0(\varepsilon)}\left[1 + \frac{1}{(1+u)^2}\right]\left(\frac{u}{u_0}\right)^{1/3} \ln\left(\frac{u_0}{u}\right)\vartheta(u_0 - u), \tag{1.15}$$

where $\vartheta(z) = 1$ for $z > 0$ and $\vartheta(z) = 0$ for $z < 0$,

$$u_0 = \frac{25}{6}\chi_s + 80\frac{1}{ma_s}\frac{\sqrt{\rho_c}}{(2 + \rho_c)}. \tag{1.16}$$

The function $r(\varepsilon)$ in Eq.(1.15) is determined by the condition of the coincidence of the total intensity

$$I_{ch}(\varepsilon) = \int_0^{\varepsilon} d\omega \left(\frac{dI_{ch}}{d\omega}\right) \tag{1.17}$$

given by Eq.(1.15) with a corresponding expression obtained in CFA (see Eq.(3.1) in [16] without corrections to CFA) for the uniform distribution over transverse coordinates. So Eq.(1.15) reproduces the energy dependence of coherent contribution to the radiation length, $L_{ch} = \varepsilon / I_{ch}(\varepsilon)$ inherent to CFA which as mentioned above is valid in a wide energy range. For the sake of possible use, we have fitted our results for the function $r(\varepsilon)$ in the energy interval $\varepsilon < 5GeV$ by a polynomial

$$r(\varepsilon) = \sum_{n=0}^{9} a_n \varepsilon^n ,$$

where ε is measured in GeV and coefficients a_n for $< 110 >$-axis of Si and Ge crystals and for $< 111 >$-axis of W crystal are given in Table in [14]. This fitting provides the accuracy better than 1 percent for Si and Ge and better than 3 percent for W.

The position of a maximum in the spectrum given by Eq.(1.15) is always consistent with the estimate Eq.(1.14). For relatively small energies when $\rho_c \ll 1$ and correspondingly $u_0 \ll 1$, we can neglect the first term in the right-hand side of Eq.(1.16) since $\rho_c / \chi_s = 2ma_s \gg 1$. In this case the spectrum Eq.(1.15) has a maximum at $\omega = \omega_{max} \simeq 0.05 \varepsilon u_0 \simeq 2\varepsilon \sqrt{\rho_c} / (ma_s)$ which evidently coincides in this (dipole) approximation with Eq.(1.14). When $\rho_c \gg 1$ and CFA is valid the spectrum Eq.(1.15) reproduces not only the position of a maximum but also the shape of spectral distributions like those shown in Fig.2 of [16] obtained within the approximation mentioned . We have compared the shape of the spectrum Eq.(1.15) with available experimental data, but this procedure is somewhat indirect for several reasons. Sometimes very thin samples were used where the distribution of electrons over transverse coordinates was far from being uniform, sometimes energy loss spectra were measured which are noticeably different from true intensity spectra, sometimes emitted photons were collimated that also results in a change of the observed shape of spectra. Nevertheless, a qualitative agreement of the spectrum Eq.(1.15) with known experimental data holds for all energies beginning with $900\, MeV$. Of course, Eq.(1.15) can not give a correct description of the coherent contribution to the radiation from particles with energies less than $100\, MeV$. Furthermore, multiple scattering is very intensified in this energy region so that particles may acquire an angle with respect to the axis noticeably exceeding θ_c. At the same time, for such energies the intensity $I_{ch}(\varepsilon)$ is already small as compared to that caused by the incoherent contribution $I_{br}(\varepsilon)$ which is always present in crystals in slightly modified form comparatively to the amorphous case. For instance, at $\varepsilon = 70\, MeV$ near $< 111 >$ axis of tungsten we have $I_{ch} / I_{br} \simeq 0.1$ and the coherent contribution can be simply neglected. Nevertheless, for the sake of consistency we shall use Eq.(1.15) at any energy up to ε_f to describe the coherent contribution to the radiation. But for the particles acquiring an angle $\theta \geq \theta_c$ owing to multiple scattering, the quantity u_0 in Eq.(1.16) will be multiplied by the factor $0.5 \sqrt{1 + (\theta / \theta_c)^2}$ according to Eq.(1.14) , since $\omega_0 \propto \theta$ at $\theta \geq \theta_c$.

Analysis of incoherent contribution to the radiation and pair-production probabilities is given in detail in [14].

The contribution to any process going on in a crystal is a sum $Y = Y_{coh} + Y_{inc}$ where, generally speaking, the incoherent contribution Y_{inc} differs from the amorphous value Y_{am}. The scale of this modification depends on the process under consideration. For the total intensity of the incoherent radiation and the quantity $\tilde{L}_{rad} = \varepsilon / I_{br}$ connected to it, the typical scale of diminishing of I_{br} as compared to I_{am} at room temperature is depending on media 9 to 13 per cent. The diminishing of the total probability of pair-production is of the same order of magnitude. In particular, for tungsten in the case of a full screening $\tilde{L}_{rad} = 1.1\, L_{rad}$. As far as the coherent contribution to the pair-production probability is negligible in the considered energy region and modifications of incoherent contributions are small, distinctions in the soft cascade development in crystal and amorphous media are mainly due to the coherent contribution to the radiation. This contribution changes the shape of photon spectra, enriching their soft part and noticeably diminishing the effective radiation length L_{ef} determined by the relation

$$L_{ef}^{-1} = \tilde{L}_{rad}^{-1} + L_{ch}^{-1}. \tag{1.18}$$

So, for the $< 111 >$ axis of tungsten, we find $L_{ef} \simeq 0.13\, cm$ at $\varepsilon = 2GeV$ and $L_{ef} \simeq 0.08\, cm$ at $\varepsilon = 5GeV$, which are several times less than the amorphous value $L_{rad} \simeq 0.35\, cm$. Thus in a crystal the initial electron is converted into photons along appreciably shorter length than in a corresponding amorphous medium, while further development of the soft shower in both media is more or less the same. Hence the most pronounced distinctions of shower characteristics in the amorphous and crystal case appear for small thicknesses. It is clear that for the valuable use of crystal properties one can utilize a hybrid target composed of crystal and amorphous layers, the former must be of a few L_{ef} thick.

In the hybrid target which consists of the crystal part followed by the amorphous one, the thickness of the crystal constituent of several L_{ef} is obviously quite enough. Indeed, at the depth $L_0 \approx (3 \div 4) L_{ef}$ most of the particles, including the initial electrons, are sufficiently soft to reduce the coherent contribution to the radiation to the level of the incoherent one. Thereby, the further development of the shower proceeds more or less in the same way for the crystal or amorphous type of the remaining part of the target. We emphasize that the crystal part $L \leq L_0$ of the target serves as the radiator, and secondary charged particles are still not so numerous at this stage of the shower development. Therefore only a small portion of the total energy loss is deposited in the crystal part of the target which considerably reduces a danger of its overheating. The softness of photon spectra is another important feature of the crystal radiator giving additional advantages for the positron production in comparison with the entirely amorphous target. To get more definite idea concerning the shape of the power spectrum one can use its explicit form given by Eq.(1.15). To present the scale, let us list some values ω_{max} where this spectrum is maximum: $\omega_{max}(1\ GeV) \simeq 31$ MeV, $\omega_{max}(4\ GeV) \simeq 170$ MeV, and $\omega_{max}(8\ GeV) \simeq 490$ MeV. Note that the width of the spectrum is typically several times larger than ω_{max}. The increase in the number of relatively soft photons turns out to be much more pronounced than that in the total radiation intensity. In the end, just this fact leads to the substantial enhancement of the positron yield from crystal targets.

To estimate the possibility of utilization of crystal targets in a positron source it is important to know not the total number of created positrons but the number of positrons in a definite phase space which can be accepted by the corresponding matching optical system. We shall use typical parameters of such system mentioned in [15], assuming that the energies of accepted positrons and their transverse (with respect to the incident beam direction) momenta must satisfy the following relation

$$5MeV \leq \varepsilon \leq 25MeV \ , \ p_{\perp} \leq 4MeV/c.$$

The number of accepted positrons N_{+}^{A} depending on the initial electron energy, the thickness and type of crystals are presented in Figs. 1-3. It is seen that the maximal yield is achieved at $L \sim 4L_{rad}$ and the maximal value increases with the atomic number, Z . The latter property is connected with the fact that with increasing Z the number of additional photons emitted by the coherent mechanism increases as well. An enlargement of the transverse momentum boundary value leads naturally to an increase of the accepted positron number and vice versa, what is illustrated by Fig.4.

The energy deposited in a target by the initial electron and created charged particles is one of the fundamental characteristics of the positron source. Because we use simplified formula for ionization energy losses, our results for the dissipated energy must be considered as the upper bound. In Fig.5 both the accepted positron yield and the deposited energy per one incident electron are presented for amorphous and crystal tungsten depending on the target thickness. It is seen that the relative gain for a crystal increases with increasing energy of initial electrons. For given number of accepted positrons N_{+}^{A}, the energy deposited ε_{dep} in a crystal sample is less than in an amorphous one.

Recently the positron production in axially aligned single crystals was studied in two series of experiments performed at CERN [19], [20] and KEK [21], [22]. The initial energy of electrons was 3 GeV [21], 6 and 10 GeV [20], 8 GeV [22], and 10 GeV [19]. In all cases the initial electron beam was aligned with the $< 111 >$ - axis of the tungsten crystal that sometimes served as the crystal part of the hybrid target which contained an additional amorphous tungsten target. A noticeable enhancement of the low-energy positron yield was observed in all experiments cited above when the yield from the crystal target was compared with that from the amorphous target of the same thickness. The experimental results and our theoretical estimations presented in the next Section display a rather good agreement with each other.

2 Comparison of theory with experiment

Theoretical results for the conditions of the experiments cited above were obtained using the approach developed in [14] and [18] where various positron and photon distributions as well as deposited energies in different crystals were calculated for the energy range of initial electrons from 2 to 300 GeV. In these papers, all the formulas used in Monte-Carlo simulations of the specific $e^{-}e^{+}\gamma$ - shower characteristics are given in the explicit form. Remember that our simplified description of the

shower development takes into account coherent (induced by the regular motion of particles in the field of crystal axes) and incoherent (like that in an amorphous medium) mechanisms of photon emission and pair production processes. The multiple scattering and the ionization energy loss of electrons and positrons are taken into account neglecting crystal effects. The coherent radiation from channeling and moving not very high above the axis potential barrier particles is described using the semi - phenomenological spectrum suggested in [14]. The corresponding computer code was developed. This allows one to calculate energy, angular, and coordinate distributions of positrons emergent from the crystal or hybrid target and to find an amount of the energy deposition. We think that the investigation of such distributions should be the main object of the experiments having the creation of the crystal assisted positron source as their ultimate aim.

2.1 Experiment (CERN) at $\varepsilon_0 = 10$ GeV

Among experiments cited above, spectral - angular distributions of created positrons were measured only in WA103 experiment at CERN (see [19], [20]) where our code was used in simulations as the event generator. This simulation allowed for the acceptance conditions and the efficiency of the detectors used. Shown in Fig.6 taken from [20] is one example of the measured and simulated distributions of positrons from 10 - GeV electrons aligned with the $< 111 >$- axis of the 8 - mm - thick crystal tungsten.

The angular acceptance conditions in WA103 experiment were approximately $|\vartheta_V^{out}| \leq 1.5°$ for the vertical and $0 \leq \vartheta_H^{out} \leq 25°$ for the horizontal angle of outgoing positron with respect to the initial electron beam direction. We shell see below that the shape of the positron spectrum depends on the degree of collimation. The one-dimensional (over ϑ_H^{out}) angular distribution is presented for positrons having energies in the $5 \div 45$ MeV range. We emphasize that the relative difference between measured and simulated results typically does not exceed 20 % in both spectral and angular distributions as seen in Fig.6. We are aware that preliminary results for another settings used in the same experiment do not contradict with the estimated scale of the difference between the data and theoretical predictions. We hope that this interrelation will not become worse after performing the complete analysis of the data which now is underway. This analysis will also give more detailed information concerning spectral - angular distributions of positrons depending on initial electron energies and target thicknesses.

2.2 Experiment (KEK) at $\varepsilon_0 = 3$ GeV

The main goal of the experiment [21] was an attempt to apply the crystal target to the working electron/positron linac, the injector for the electron - positron collider B - Factory at KEK. Thus, the acceptance conditions for created positrons were determined by the momentum acceptance of the positron linac with the matching section which is 8.2 MeV/c $< p <$ 11.6 MeV/c and $p_\perp <$ 2.4 MeV/c. The hybrid target used consists of 1.7 - mm - thick tungsten crystal followed by 7 - mm - thick

amorphous tungsten. The observed positron yield was enhanced by the factor 1.40 when the $< 111 >$ crystal axis was aligned with 3 GeV incident electron beam as compared to the case of the disoriented crystal. Our number for this enhancement is 1.47 being only 5 % larger than the experimental one. Note that in the experiment [21] the crystal and amorphous parts of the hybrid target were separated by the distance of 70 mm. This circumstance, which, in principle, may slightly change the enhancement value, was not taken into account in our calculation. Recollect that the amount of the energy deposited in the crystal part (ε_{dep}^{cr}) of the hybrid target may be much smaller than that (ε_{dep}^{am}) in the amorphous one. Such interrelation of ε_{dep}^{cr} and ε_{dep}^{am} should take place in the case of [21], where the crystal thickness is about 1.8 L_{ef} (see discussion in the Introduction). This is confirmed by our calculations which give $\varepsilon_{dep}^{cr} \simeq 11$ MeV and $\varepsilon_{dep}^{am} \simeq 277$ MeV per one incident electron.

2.3 Qualitative features of positron distributions and experiment (KEK) at $\varepsilon_0 = 8$ GeV

In [22] the positron production efficiency from 2.2 - mm, 5.3 - mm and 9.0 - mm - thick tungsten crystals was measured using an 8 - GeV electron beam. Positrons produced in the forward direction with momenta 10, 15 and 20 MeV/c were detected by the magnetic spectrometer. Thus, only several points in the energy distribution were determined under hard collimation conditions. Therefore, before going on to the comparison of the experimental results with our, let us remind some important qualitative features of spectral - angular distributions using 8 GeV electrons and the $< 111 >$ - axis of the tungsten crystals as an example. For the sake of comparison, the corresponding distributions for amorphous tungsten will be presented as well. Below all the quantities characterizing the positron yield are normalized per one incident electron.

The use of matching systems implies some collimation (typically $\vartheta_{out} \leq 25°$) of outgoing positrons. Shown in Fig.7 is the energy dependence (energy step is equal to 10 MeV) of the positron yield from crystal (a) and amorphous (b) targets of the same thickness $L = 2.2$ mm. In the case of the hard collimation, when $\vartheta_{out} \leq 1°$ (open circles), the yield is multiplied by 10 to make it visible. The larger the positron energy, the smaller is the typical value of ϑ_{out} since both production and multiple scattering processes are characterized by smaller angles for higher energies. This is seen in Fig.7 (a) where the spectral curves for $\vartheta_{out} < 180°$ and that for $\vartheta_{out} \leq 24°$ are overlapping within precision better than 1 % starting from $\varepsilon_{cr}^{(1)} \simeq 55$ MeV. In turn, from $\varepsilon_{cr}^{(2)} \simeq 110$ MeV the same happens with curves corresponding to $\vartheta_{out} \leq 24°$ and $\vartheta_{out} \leq 12°$. Such behavior is also seen in Fig.7 (b) for the amorphous target where $\varepsilon_{am}^{(1)} \simeq 50$ MeV and $\varepsilon_{am}^{(2)} \simeq 105$ MeV. In other words, positrons with energies $\varepsilon > \varepsilon^{(1)}$ are practically concentrated within the cone $\vartheta_{out} \leq 24°$ and those with $\varepsilon > \varepsilon^{(2)}$ have $\vartheta_{out} \leq 12°$. In accordance with this picture, the spectral maximum is shifted to the right while the width of the distribution increases when the collimation angle decreases. The enhancement μ, being bin-by-bin ratio of the positron yield from the crystal target to that from the amorphous one at the same collimation, is almost constant for $\varepsilon < 45$ MeV and monotonically

decreases with growing positron energy. This means that positron spectra from the crystal target are softer. Somewhat lower values of $\varepsilon^{(1)}, \varepsilon^{(2)}$ in the amorphous case point at the same feature. For given collimation, the variation of the enhancement is about 20 % over the whole energy interval presented in Fig.7. The maximum values of the enhancement at different collimation are $\mu_{max}(\vartheta_{out} \leq 180°) \simeq 6.09$, $\mu_{max}(\vartheta_{out} \leq 24°) \simeq 5.92$, $\mu_{max}(\vartheta_{out} \leq 12°) \simeq 5.67$, and $\mu_{max}(\vartheta_{out} \leq 1°) \simeq 5.29$. Apparently, they diminish as the collimation angle does so. Shown in Fig.8 is the same as in Fig.7 but for the target thickness $L = 9.0$ mm. The yield at $\vartheta_{out} \leq 1°$ (open circles) is multiplied now by 30. The qualitative behavior of spectra depending on the collimation angle at $L = 9.0$ mm is the same as at $L = 2.2$ mm. However, all the spectra become softer for the larger target thickness. This is indicated already by the increase in $\varepsilon^{(1)}$, $\varepsilon^{(2)}$ values which are now $\varepsilon^{(1)}_{cr} \simeq 85$ MeV, $\varepsilon^{(2)}_{cr} \simeq 185$ MeV, $\varepsilon^{(1)}_{am} \simeq 75$ MeV, $\varepsilon^{(2)}_{am} \simeq 165$ MeV. It is clear that the magnitude of the yield from the thicker target is essentially larger but this increase is different in the crystal and amorphous cases. For example, in the energy range $\varepsilon < 45$ MeV the yield is increased by $6 \div 7$ times for a crystal and by $17 \div 20$ times for amorphous samples. As a result, the enhancement at $L = 9.0$ mm is almost 3 times less than at $L = 2.2$ mm in this energy range. At $L = 9.0$ mm the enhancement is peaked in the first bin ($\varepsilon \in (5 \div 15)$ MeV) for every collimation. Its maximum values are $\mu_{max}(\vartheta_{out} \leq 180°) \simeq 2.25$, $\mu_{max}(\vartheta_{out} \leq 24°) \simeq 2.15$, $\mu_{max}(\vartheta_{out} \leq 12°) \simeq 2.08$, and $\mu_{max}(\vartheta_{out} \leq 1°) \simeq 2.06$. The enhancement monotonically decreases with growing positron energy and approximately halves at $\varepsilon \approx 250$ MeV. Thus, positron spectra from the crystal target are softer at $L = 9.0$ mm as well, and this property is much more pronounced in comparison with $L = 2.2$ mm.

Matching systems can be characterized also by the maximum transverse momentum $p_\perp^{max}$ of accepted positrons. In this connection, spectra of positrons having $p_\perp < p_\perp^{max}$ are of definite interest. Such spectra at $L = 2.2$ mm (a) and at $L = 9.0$ mm (b) from crystal and amorphous targets are shown in Fig.9. In contrast to the case of the pure angular selection (cf. Figs.7,8 the position of spectral maxima at limited $p_\perp$ values is always in the first bin ($\varepsilon \in (7.5 \div 12.5)$ MeV). Corresponding maximum values are $\mu_{max}(5\ MeV/c) \simeq 5.82$, $\mu_{max}(2.5\ MeV/c) \simeq 5.62$ at $L = 2.2$ mm and $\mu_{max}(5\ MeV/c) \simeq 2.17$, $\mu_{max}(2.5\ MeV/c) \simeq 2.11$ at $L = 9.0$ mm. The enhancement monotonically decreases with growing positron energy. Its variation over the whole energy interval presented in Fig.9 is about 15 % at $L = 2.2$ mm and 40 % at $L = 9.0$ mm. So, for this selection too, positron spectra from crystal targets are softer than those from amorphous targets of the same thickness. The interesting feature of spectral curves in Fig.9 is the similarity of those obtained for two different values of $p_\perp^{max}$ from the same target. The scaling factors η are $\eta_{cr} \simeq 2.6$, $\eta_{am} \simeq 2.5$ at $L = 2.2$ mm and $\eta_{cr} \simeq 3.1$, $\eta_{am} \simeq 3.0$ at $L = 9.0$ mm. These factors turn out to be practically (within an accuracy of a few percent) independent of the total positron momentum p. This fact can be easily understood if we assume that the width of the angular distribution of positrons is completely due to multiple scattering being, thereby, proportional to p^{-1}. Such assumption is confirmed by results of the calculation shown in Fig.10 for two groups of positrons. One of them contains positrons having momentum in the interval $p \in (8.5 \div 11.5)$ Mev/c , for

another group $p \in (17 \div 23)$ Mev/c.

For the given target, the width of the angular distribution of positrons with $p \approx$ 10 Mev/c is approximately twice as much that for $p \approx 20$ Mev/c as expected. The width of every distribution evidently increases when we go on to the thicker target of the same kind. Comparing angular distributions from crystal and amorphous targets of the same thickness, we find that at $L = 9.0$ mm the distributions are somewhat (about 1.5°) wider in the crystal case for both groups. In units of FWHM of the distribution from the crystal target these differences are about 6.5 % at $p \approx 10$ Mev/c and 14 % at $p \approx 20$ Mev/c. At $L = 2.2$ mm the distribution from the crystal target is wider by 15.5 % at $p \approx 20$ Mev/c whereas this is narrower by 10 % at $p \approx 10$ Mev/c.

Going on to the comparison of our results with those obtained in [22], let us remind that to perform an accurate comparison of such kind, exact information is needed concerning the acceptance conditions and registration efficiency of detectors in the experiment. As noted in [22], at $p = 20$ Mev/c, the momentum acceptance ($\Delta p/p$) was 3 % (FWHM) and the polar angle acceptance was less than 20 mrad (FWHM). Since the shape of the acceptance curves was unavailable to us, we have tried to simulate experimental conditions using the same angular collimation $\vartheta_{out} \leq \vartheta_{out}^{max}$ and the same value of $\Delta p/p$ for all momenta and targets. So, at the calculation of the magnitude of positron production efficiency (PPE), we simply put ϑ_{out}^{max} to 20 mrad. The value of $\Delta p/p$ was chosen to reproduce at applied collimation the experimental magnitude of PPE for the 9.0 - mm - thick amorphous target. Acting in this way, we have got $\Delta p/p = 3.2$ %. We realize that our regard for the acceptance conditions is rather rough. An additional inaccuracy was introduced when we determined the PPE numbers from Fig.10 of [22]. Note that the experimental numbers obtained in a such way, which are presented by filled symbols in Fig.11, do not reproduce exactly the whole set of mean experimental values for the enhancement given in Table 1 of [22]. Moreover, in Fig.10 of [22] there are no experimental points for 2.2 and 5.3 - mm - thick amorphous targets. For these two cases, we present in Fig.11 the values of PPE given by smooth - curve fits corresponding to simulation fitting in Fig.10 of [22]. Bearing all this in mind, we, nevertheless, can assert that a rather good agreement is seen in Fig.11 of the experimental results and our estimations. Relative difference of them is better than 13 % everywhere except the values of PPE at $p = 10$ and 15 Mev/c from both thinnest ($L = 2.2$ mm) targets, where the experimental yield is underestimated by 19 % to 42 %. Note that just for this thickness the largest inaccuracy was introduced while determining the PPE numbers from Fig.10 of [22] at $p = 10$ and 15 Mev/c, as the magnitude of the yield is especially small in this case.

In contrast to the magnitude of the positron yield, the enhancement is not very sensitive to the acceptance conditions. The calculated values of the enhancement(theory) are presented in Table 2 along with those taken from Table 1 of [22] (experiment). Purely statistical errors are figured in Table 2 as theoretical ones. The relative error in PPE was estimated as $N_{ef}^{-1/2}$, where N_{ef} is the mean number of events in the phase space corresponding to the acceptance conditions used in calculations. The total statistics was chosen so that approximately to equalize values

Table 2: Enhancement of the positron yield from crystal targets

Momentum (MeV/c)	Enhancement (2.2-mm-thick)		Enhancement (5.3-mm-thick)		Enhancement (9.0-mm-thick)	
	theory	experiment	theory	experiment	theory	experiment
10	6.0 ± 0.5	6.5 ± 0.6	3.2 ± 0.3	3.4 ± 0.7	2.1 ± 0.2	2.3 ± 0.4
15	5.5 ± 0.3	6.2 ± 0.8	3.2 ± 0.2	3.2 ± 0.5	2.0 ± 0.1	2.0 ± 0.2
20	5.4 ± 0.2	5.1 ± 0.5	2.9 ± 0.1	3.0 ± 0.5	1.8 ± 0.1	1.8 ± 0.2

of N_{ef} for amorphous and crystal targets of the same thickness. At given total statistics, the quantity N_{ef} increases with growing positron momentum in accord with a shape of the positron spectra at hard collimation shown in Figs. 2,3. This fact leads to a better statistical accuracy for larger momentum. We emphasize that the differences of the estimated and experimental enhancement values are smaller than corresponding experimental errors for all momenta and samples figured in Table 2.

3 Conclusion

Using the simple computer code suggested in [14] and [18], we have compared the theoretical predictions for some characteristics of the electromagnetic shower developing in axially aligned crystals with experimental results reported in [19],[20] and [21],[22]. On the whole, theory and experiment are consistent within the experimental accuracy. From this comparison we also conclude that the accuracy provided by the existing simplified code is at least better than 20%. This accuracy may be slightly improved if we include into consideration some processes like annihilation of positrons or Compton scattering of photons which were ignored as corresponding cross sections are small in the energy region of interest. However, the approximate character of the radiation spectra at axial alignment used in our calculations still provides the main theoretical uncertainty. Nevertheless, we believe that the level of the accuracy already achieved in the theoretical description is quite sufficient to make a reliable choice for optimal parameters of the positron source using axially aligned single crystals.

Acknowledgments We are grateful to Prof. H.Okuno for providing us with details of the experiment [22] and to the authors of [20] for numerous fruitful discussions. Support of this work by the Russian Fund of Basic Research under Grants 00-02-18007, 01-02-16926, and 00-02-22003 is also gratefully acknowledged.

References

[1] V.N.Baier, V.M.Katkov and V.M.Strakhovenko, phys.stat.sol.(b)**133** (1986) 583.

[2] V.N.Baier, V.M.Katkov and V.M.Strakhovenko, Phys. Lett. A, **95** (1983) 403.

[3] V.N.Baier, V.M.Katkov and V.M.Strakhovenko, Nucl. Instr. and Meth. B **4** (1984) 346.

[4] V.N.Baier, V.M.Katkov and V.M.Strakhovenko, Sov.Phys.Dokl. **29** (1984) 306.

[5] V.N.Baier, V.M.Katkov and V.M.Strakhovenko, Phys. Lett. A, **162** (1992) 429.

[6] V.N.Baier, V.M.Katkov and V.M.Strakhovenko, phys.stat.sol.(b)**149** (1988) 403.

[7] V.N.Baier and R.Chehab, Positron Source based on Channeling Radiation, Proposal for an Experiment at Orsay, LAL, Orsay, France (May 1990).

[8] V.N.Baier, V.M.Katkov and V.M.Strakhovenko, Sov. Phys. Usp. **32** (1989) 972.

[9] V.N.Baier, V.M.Katkov and V.M.Strakhovenko, *Electromagnetic Processes at High Energies in Oriented Single Crystals*, World Scientific Publishing Co, Singapore, 1998.

[10] V.N.Baier, V.M.Katkov and V.M.Strakhovenko, Nucl. Instr. and Meth. A **250** (1986) 514.

[11] V.N.Baier, V.M.Katkov and V.M.Strakhovenko, Nucl. Instr. and Meth. B **27** (1987) 360.

[12] R.Medenwaldt et al.,Phys. Lett. B **227** (1989) 483.

[13] V.N.Baier, V.M.Katkov and V.M.Strakhovenko, Nucl. Instr. and Meth. B **119** (1996) 131.

[14] V.N.Baier, V.M.Katkov and V.M.Strakhovenko, Nucl. Instr. and Meth. B **103** (1995) 147.

[15] X.Artru, V.N.Baier, R.Chehab, and A.Jejcic, Nucl. Instr. and Meth. A **344** (1994) 443.

[16] V.N.Baier, V.M.Katkov and V.M.Strakhovenko, Sov.Phys.JETP, **65** (1987) 686.

[17] V.N.Baier, V.M.Katkov and V.M.Strakhovenko, phys.stat.sol.(b)**149** (1988) 403.

[18] V.N.Baier and V.M.Strakhovenko, Nucl. Instr. and Meth. B **155** (1999) 403.

[19] R.Chehab et al. Proceedings of LINAC2000, Monterey, CA, USA, August 2000, p.143

[20] R.Chehab et al. Phys. Lett. B, **525** (2002) 41.

[21] M.Inoue, S.Takenaka, K.Yoshida et al, Nucl. Instr. and Meth. B **173** (2001) 104.

[22] H.Okuno et al. Report on RREPS-01 Conference, Lake Aya, Russia, September 2001; KEK Preprint 2001-146.

Figure captions.

Fig.1. Number of accepted positrons N_+^A versus crystal thickness L in Si near $< 110 >$-axis . The initial electron energy (in GeV) is indicated near corresponding curves.

Fig.2. The same as in Fig.1 but for Ge near $< 110 >$-axis .

Fig.3. The same as in Fig.1 but for W near $< 111 >$-axis .

Fig.4. Number of positrons having energies in the interval $5 \div 25 MeV$ versus thickness of tungsten crystal for different values of boundary transverse momentum $p_\perp$ indicated (in MeV/c) near corresponding curves.

Fig.5. Number of accepted positrons N_+^A (curves 3,4) and deposited energy ε_{dep} (curves 1,2) for $\varepsilon_i = 5GeV$ in amorphous (curves 1,3) and crystal (curves 2,4) tungsten depending on the thickness L.

Fig.6. Spectral (left) and angular (right) distributions of positrons from 10 GeV electrons traversing 8 - mm - thick crystal tungsten target along the $< 111 >$- axis. Open circles: simulation, filled circles: experiment.

Fig.7. Positron yield depending on energy from 2.2 - mm - thick crystal (a) and amorphous (b) targets at different collimation. Filled triangles - no collimation ($\vartheta_{out} \leq 180°$), open triangles - $\vartheta_{out} \leq 24°$, filled circles - $\vartheta_{out} \leq 12°$, and open circles - $\vartheta_{out} \leq 1°$ (multiplied by 10).

Fig.8. Positron yield depending on energy from 9.0 - mm - thick crystal (a) and amorphous (b) targets at different collimation. Filled triangles - no collimation ($\vartheta_{out} \leq 180°$), open triangles - $\vartheta_{out} \leq 24°$, filled circles - $\vartheta_{out} \leq 12°$, and open circles - $\vartheta_{out} \leq 1°$ (multiplied by 30).

Fig.9. Positron yield depending on energy at $L = 2.2$ mm (a) and $L = 9.0$ mm (b) for $p_\perp^{max} = 2.5$ MeV/c (curves 1 and 3) and for $p_\perp^{max} = 5$ MeV/c (curves 2 and 4). Solid curves represent the yield from crystal and dotted from amorphous targets.

Fig.10. Angular distribution $dN^{(+)}/d\Omega$ depending on outgoing positron angle at $L = 2.2$ mm (a) and at $L = 9.0$ mm (b) for $p \in (8.5 \div 11.5)$ Mev/c (curves 1 and 3) and for $p \in (17 \div 23)$ Mev/c (curves 2 and 4). Solid curves represent the yield from crystal and dotted from amorphous targets.

Fig.11. Positron production efficiency from crystal (a) and amorphous (b) targets depending on thickness. Open symbols - our calculation, filled symbols - results from Fig.5 of [22]; open triangles are for $p = 20$ Mev/c, open circles are for $p = 15$ Mev/c, and open squares are for $p = 10$ Mev/c.

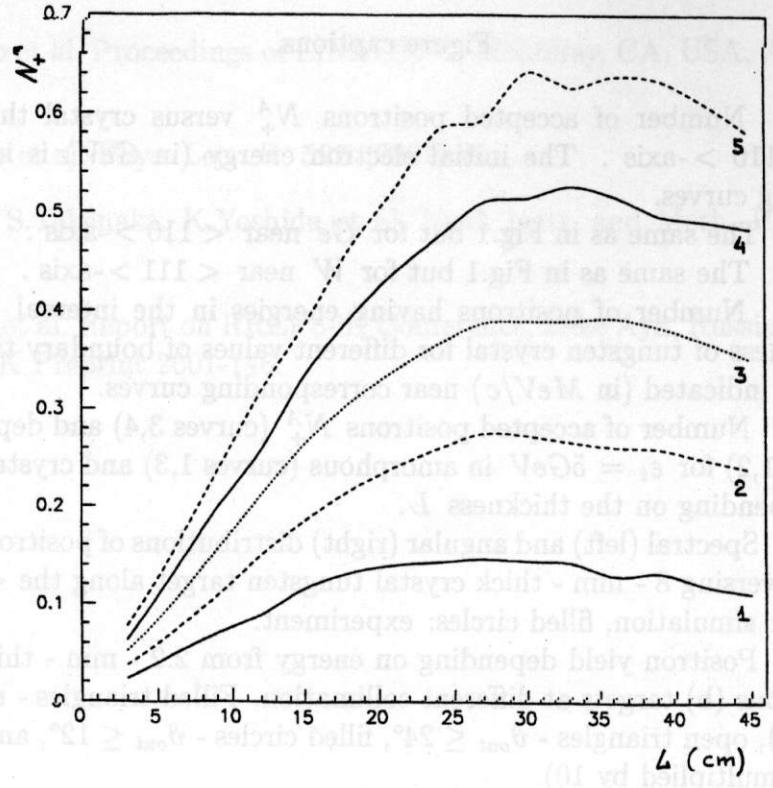
0.7
0.6
0.5
0.4
0.3
0.2
0.1
0
0
5
10
15
20
25
30
35
40
45
L (cm)
1
2
3
4
5

Fig. 1

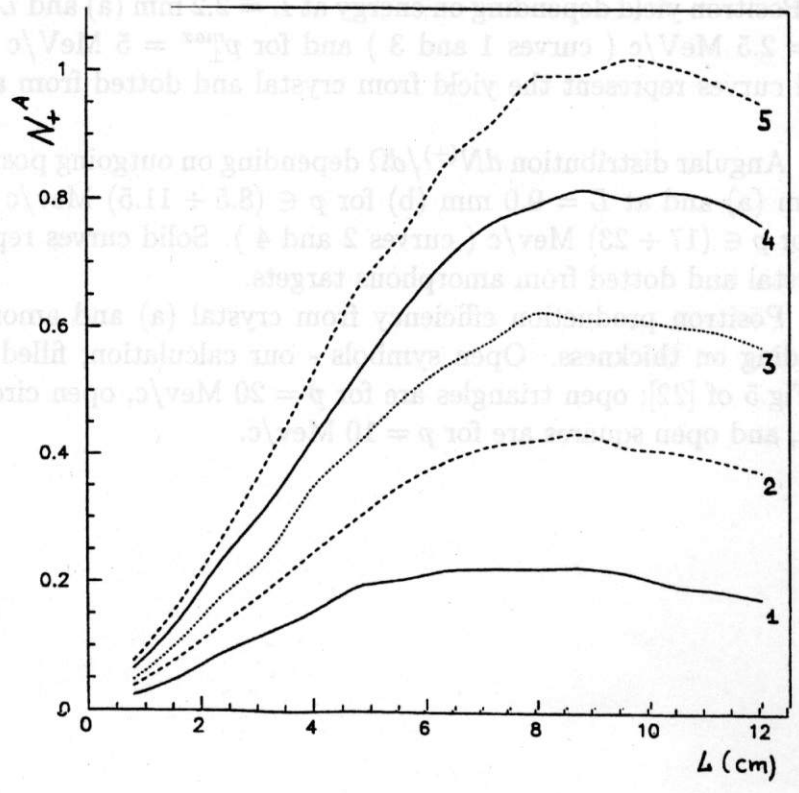
1
0.8
0.6
0.4
0.2
0
0
2
4
6
8
10
12
L (cm)
1
2
3
4
5

Fig. 2

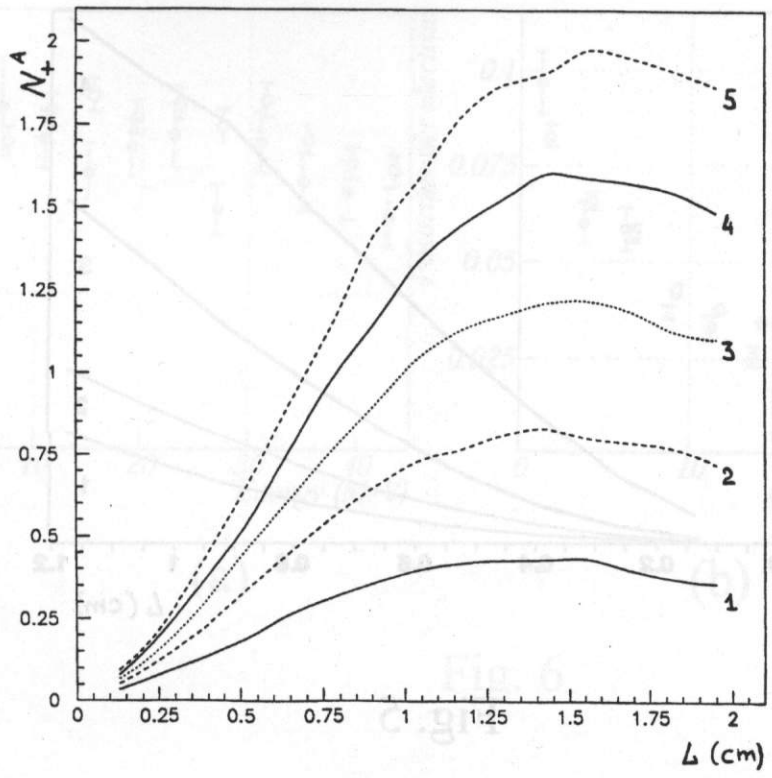
N_+^A
2
1.75
1.5
1.25
1
0.75
0.5
0.25
0
0
0.25
0.5
0.75
1
1.25
1.5
1.75
2
L (cm)
5
4
3
2
1

Fig. 3

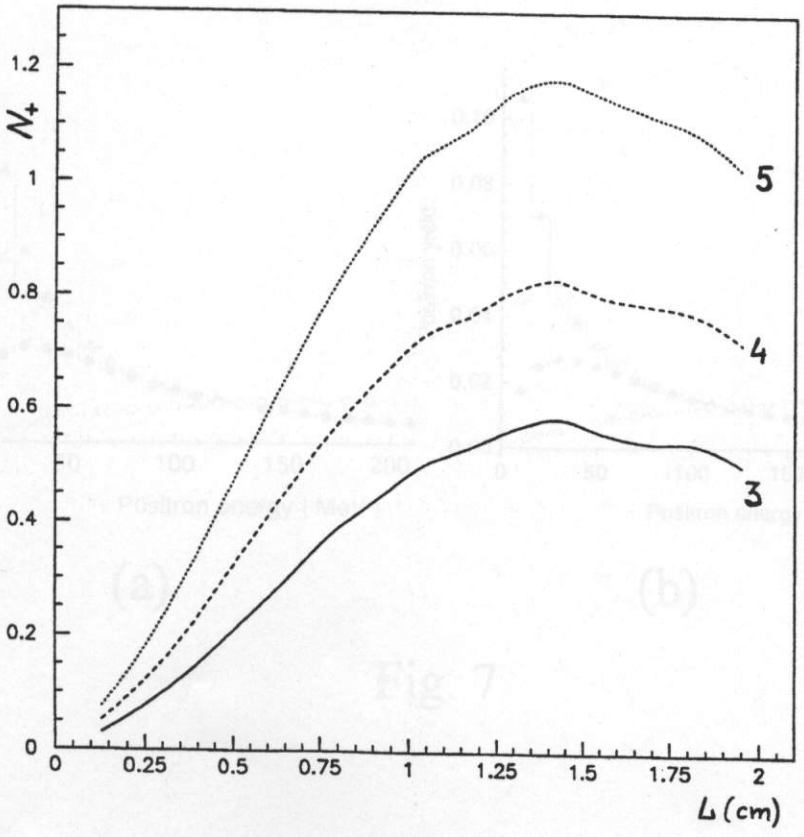
N_+
1.2
1
0.8
0.6
0.4
0.2
0
0
0.25
0.5
0.75
1
1.25
1.5
1.75
2
L (cm)
5
4
3

Fig. 4

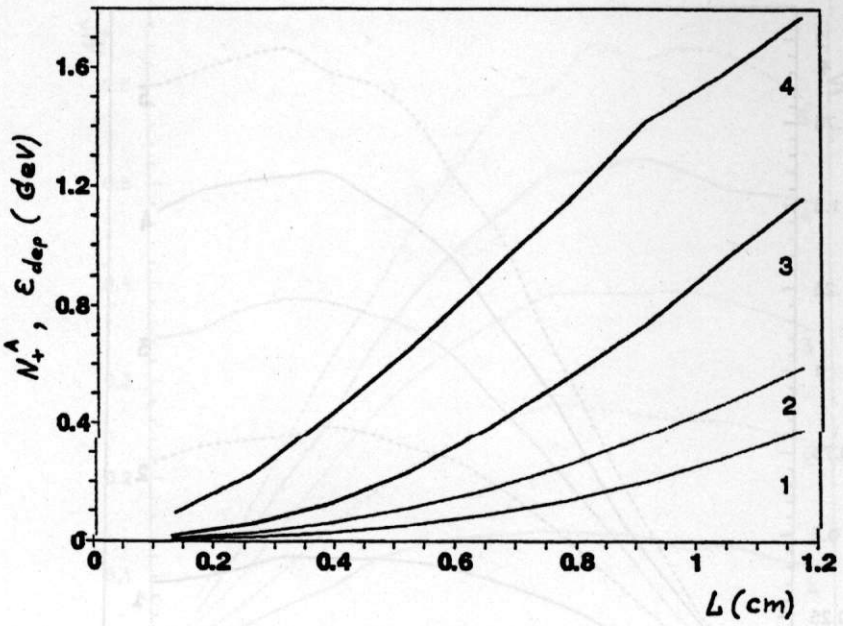

Fig. 5

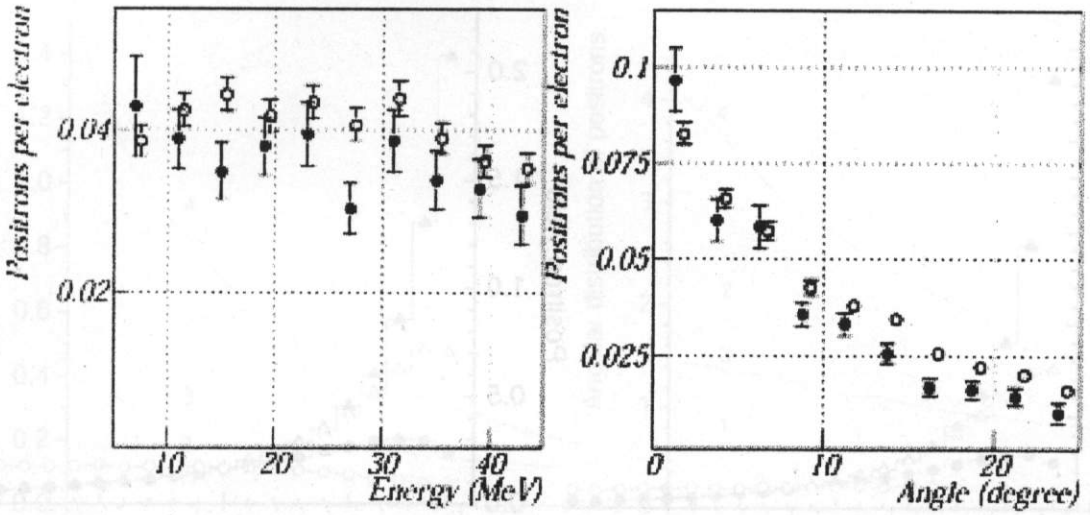

(a) (b)

Fig. 6

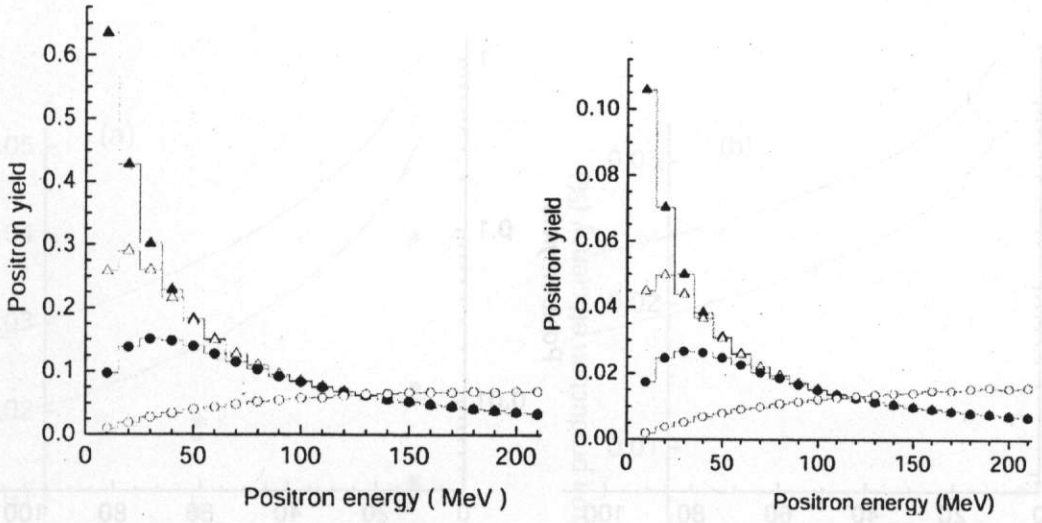

(a) (b)

Fig. 7

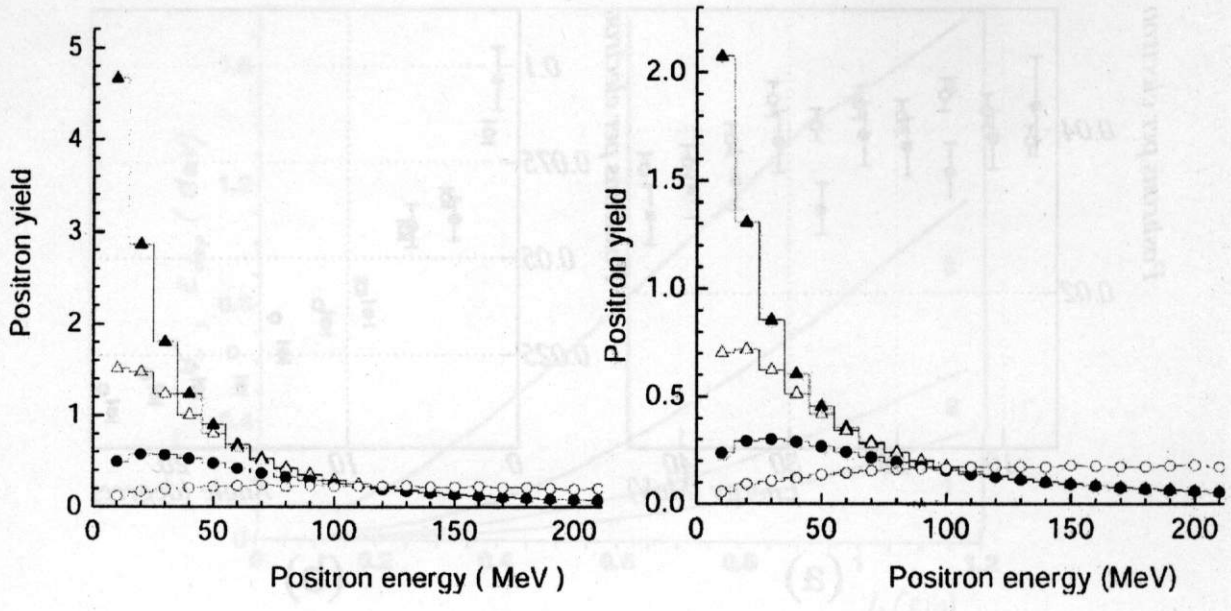

(a) (b)

Fig. 8

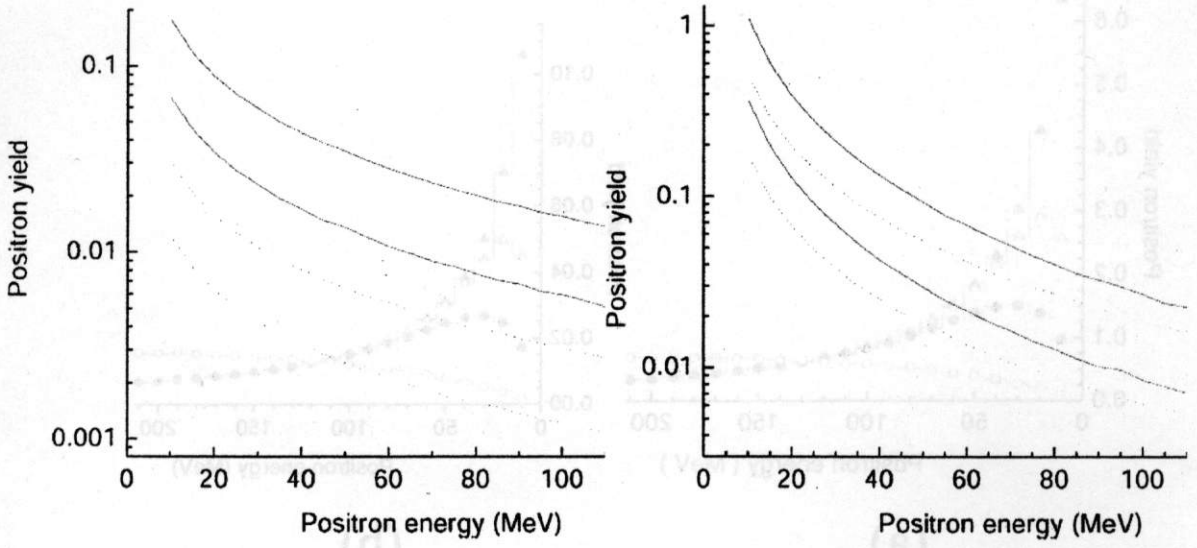

(a) (b)

Fig. 9

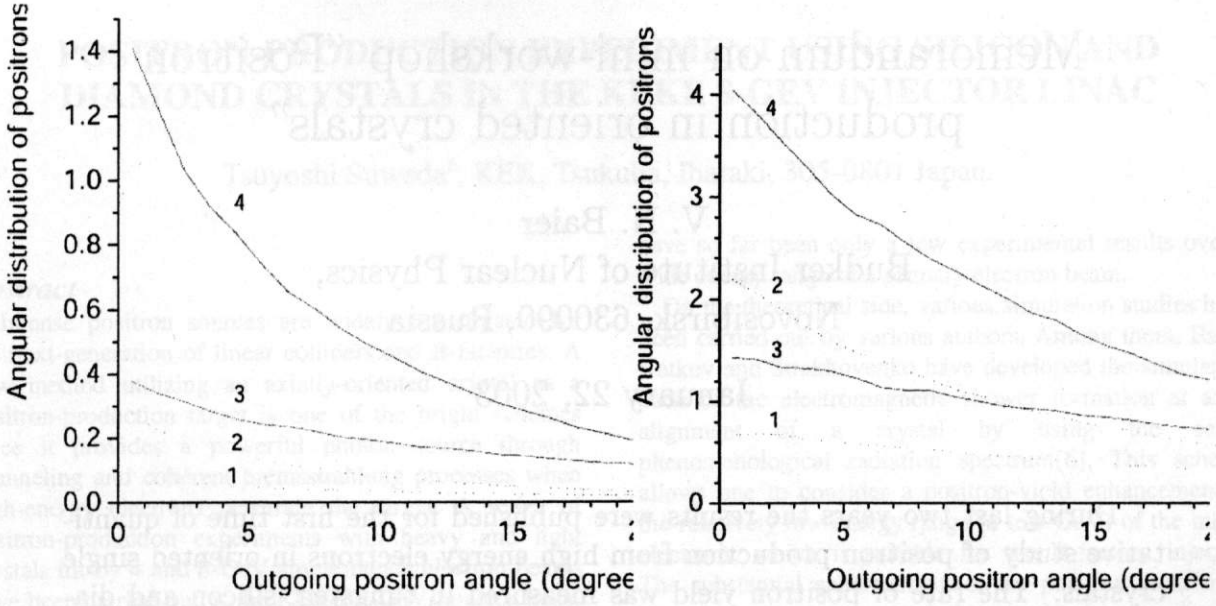
Angular distribution of positrons
Outgoing positron angle (degree
4
3
2
1
(a)
(b)

Fig. 10

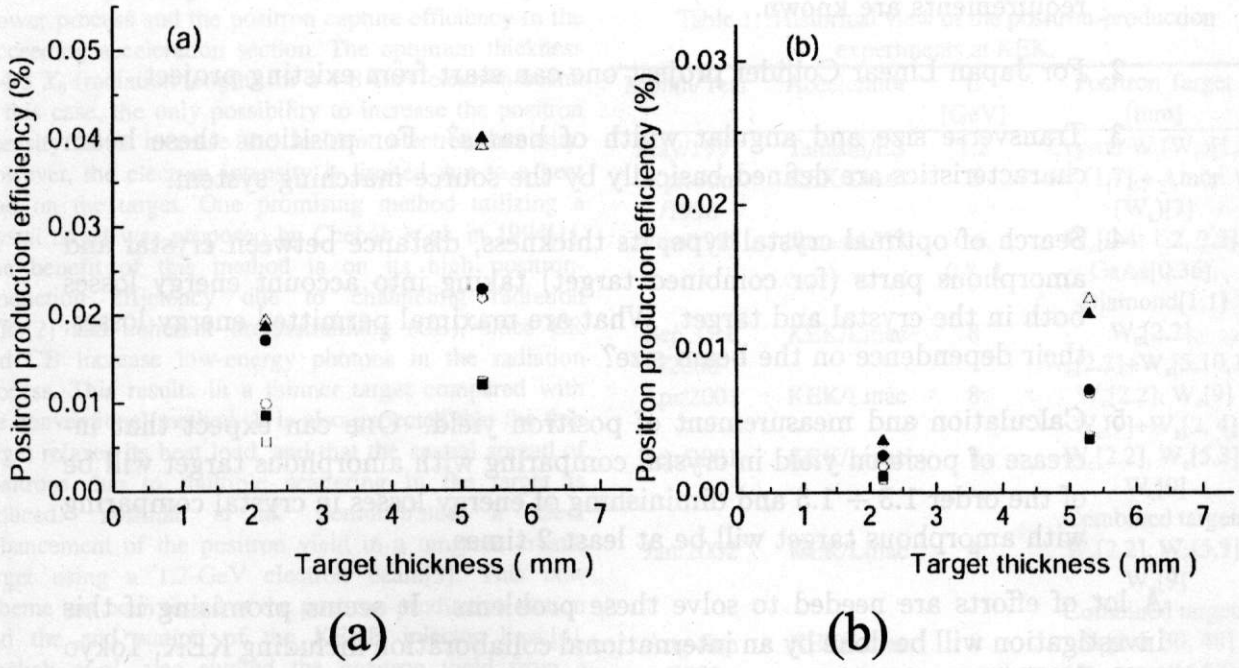
(a)
(b)
Positron production efficiency (%)
Target thickness (mm)

Fig. 11

Memorandum on mini-workshop "Positron production in oriented crystals"

V. N. Baier
Budker Institute of Nuclear Physics,
Novosibirsk, 630090, Russia

January 22, 2003

During last two years the results were published for the first time of quantitative study of positron production from high energy electrons in oriented single crystals. The rate of positron yield was measured in tungsten, silicon and diamond axially oriented crystals with accuracy of order $15 \div 20\%$. The obtained data are in quite satisfactory agreement with the theory and based on this theory simulation. This may be considered as a summary of reports presented at mini-workshop.

In my opinion this means that now is just a time to make the next step and start investigation of optimization of the positron source. This includes:

1. Reasonable definition of needed intensity of positron source. What is the optimal energy both for electron and positron? For KEKB factory the current requirements are known.

2. For Japan Linear Collider project one can start from existing project.

3. Transverse size and angular width of beams? For positions these beam characteristics are defined basically by the source matching system.

4. Search of optimal crystal type, its thickness, distance between crystal and amorphous parts (for combined target) taking into account energy losses both in the crystal and target. What are maximal permitted energy losses, their dependence on the beam size?

5. Calculation and measurement of positron yield. One can expect that increase of positron yield in crystal comparing with amorphous target will be of the order $1.3 \div 1.5$ and diminishing of energy losses in crystal comparing with amorphous target will be at least 2 times.

A lot of efforts are needed to solve these problems. It seems promising if this investigation will be done by an international collaboration including KEK, Tokyo MU, BINP(Novosibirsk), ...

The specific features of the radiation under consideration, which occurs for electrons moving in a continuous potential of the axes (planes), are dictated by the particles which are in the channel and are not too high above the barrier. The contribution of these particles can be enhanced by a photon collimator. For this purpose, the collimation angle ϑ_{col} (we count it from the axis oriented to the centre of the collimator) should be chosen approximately equal to the Lindhard angle $\vartheta_{col} \approx \vartheta_c$. On the other hand, if $\vartheta_{col} < m/\varepsilon \equiv 1/\gamma$, we shall omit a fraction of the radiation of interest. For energies from several hundreds of MeV to several GeV considered, we have $\vartheta_s \gg 1/\gamma$ and $\vartheta_s \gg \vartheta_c$ at a crystal thickness $L \approx L_0$. Thus, the condition

$$\max\left(\frac{1}{\gamma}, \vartheta_c\right) \lesssim \vartheta_{col} \ll \vartheta_s \tag{4}$$

assumed to be satisfied and then the factor $\exp\left(-r_\perp^2/g(l)\right)$ can be substituted for unity[3] for particles whose radiation reaches the collimator, and the distribution proves to be uniform in a transverse phase space. As a consequence, for the intensity of the radiation under consideration (labelled by "ch") at the depth l we have

$$\frac{dI_{ch}}{d\Omega} = \frac{I}{\pi g(l)}, \tag{5}$$

where $I = \int I(x)\,dx/d_{pl}$ for the plane and $I = \int I(\varrho)\,d^2\varrho/S$ for the axis. It is worth noting that I coincides with I_{as}, the asymptotic value achieved by the intensity at the incident angles $\vartheta_0 \gtrsim \vartheta_c$ and $\vartheta_0 \gg \vartheta_c$ for the axial and planar cases, respectively. Emphasize that (5) incorporates the radiation from all the particles rather than from the above-barrier ones only. The appearance of I_{as} in (5) is due to the uniformity of the distribution in transverse phase space under the indicated assumptions, see (4), while the uniformity of the distribution with respect to $r_\perp$ resulted, in (5), in a uniform distribution with respect to the solid angle of emitted photons for the angles $\vartheta_{ph} \lesssim \vartheta_s$.

The values of $I = I_{as}$ are readily calculated for any potential of the axes, or planes. For the potentials used, an explicit expression for I_{as} is given by formulae (29) in [1, 2]. Thus, the axial potential has been taken in the form (see [5, 6])

$$U(x) = V_0\left[\ln\left(1 + \frac{1}{x + \beta}\right) - \ln\left(1 + \frac{1}{x_0 + \beta}\right)\right]. \tag{6}$$

For it,

$$I = I_{as} = I_0 q(\beta), \tag{7}$$

where

$$I_0 = \frac{8\pi e^2 V_0^2 \varepsilon^2}{3m^4}\, n_\perp, \qquad q(\beta) = (1 + 2\beta)\ln\left(1 + \frac{1}{\beta}\right) - 2. \tag{8}$$

In (6), $x = \varrho^2/a_s^2$ where a_s is the screening radius and the parameter β is proportional to the squared amplitude of thermal vibrations. In [6, 1] we took $V_0 = Ze^2/d$ where d is the average distance between the atoms in the chain, and the parameters β and a_s were determined by means of the fitting procedure described in [6]. Their values for the ⟨100⟩ axis of some substances are listed in the tables of [6, 1]. For the ⟨111⟩ axis, we have made a three-parametric fitting: the quantity V_0 is regarded to be a fitting parameter as well. The results of this procedure are illustrated in Table 1.

phys. stat. sol. (b) 133, 583 (1986)

Subject classification: 61.80 and 78.70; S1.1; S1.2; S5; S5.11; S5.12

Institute of Nuclear Physics, Academy of Sciences of the USSR, Novosibirsk[1])

Radiation Yield of High-Energy Electrons in Thick Crystals

By

V. N. Baier, V. M. Katkov, and V. M. Strakhovenko

1. Description of Radiation in Thick Crystals

According to the performed analysis [1, 2] dealing with the kinetics of the distribution, which is due to multiple scattering, the DF for large depths (l) is of the form

$$dF^{pl}(r_\perp, x, l) = \frac{dx}{d_{pl}}\frac{d^2v_\perp}{\pi g(l)}\exp\left(-\frac{v_\perp^2}{g(l)}\right)$$
$$dF^{ax}(r_\perp, \varrho, l) = \frac{d^2\varrho}{S}\frac{d^2v_\perp}{\pi g(l)}\exp\left(-\frac{v_\perp^2}{g(l)}\right) \tag{1}$$

where x, $y(\varrho)$ are the transverse coordinates: $|x| \leqq d_{pl}/2$ for the planar case and $|\varrho| \lesssim r_0$ for the axial case; $S = \pi r_0^2$ is the area of a cell in the transverse plane which contains the projection of one atomic chain, and $n_\perp = 1/S$ is the density of the chains of atoms (axes). The quantity $g(l)$ has the form

$$g(l) = \Delta^2 + \int_0^l \dot{\vartheta}_s^2(t)\,dt, \tag{2}$$

where $\dot{\vartheta}_s^2$ is the rate of variation of the squared angle of multiple scattering in an appropriate amorphous medium. The time (depth) dependence of $\dot{\vartheta}_s^2$ is connected with the variation of the particle energy because of radiation losses. The first term in $g(l)$ reflects the character of the angular (velocity) distribution established at the initial stage of electron motion in a crystal which depends on the angular (over ϑ_0) distribution in an incident beam. Even with the angle of incidence $\vartheta_0 = 0$, the angular spread of particles in the crystal proves to be roughly equal to the Lindhard angle: $\vartheta_c = \sqrt{2U_0/\varepsilon}$ (U_0 is the depth of the potential well and ε is the energy of a particle); therefore, assuming the incident beam to be rather narrow, $\vartheta_0 \leqq \vartheta_c$, we can put $\Delta^2 = c_1\vartheta_c^2$, where c_1 is a coefficient of the order of unity. The magnitude of c_1 can be influenced also by the imperfectness

BKS NIM B 103 (1995) 147

Here we consider axial alignment when θ_0 with respect to the chosen axis is not too large as compared to the critical (Lindhard) angle $\theta_c = (2V_0/\varepsilon)^{1/2}$,where V_0 is a typical scale of the corresponding potential and ε is the particle energy, since in this case the most pronounced effects take place.

Let us start with the coherent contribution to the radiation. As already mentioned, at sufficiently high energies corresponding expressions valid at any angle of incidence θ_0 were obtained in BKS(1987). For $\theta_0 \ll V_0/m$ they reproduce CFA-limit. But even if the initial electron energy is high enough to apply mentioned description, charged particles arising in the course of a shower development may not satisfy this condition. In the case of a soft cascade we have to describe the radiation from these "soft" particles as well. Let us remind that within semiclassical theory of the QED- processes in any external field there are only two parameters: ρ and χ. The parameter ρ is a measure of the particle velocity deviation from a straight line in units of the natural emission angle $\gamma^{-1} = m/\varepsilon$, while the parameter χ being the ratio of the external field strength in the particle rest system to the critical QED-value $E_c = 1.32 \cdot 10^{16}\, eV/cm$ is responsible for the magnitude of quantum recoil effects. In crystals

$$\chi \sim \chi_s = V_0\varepsilon/m^3a_s\,,$$

esides the radiation under study, the bremsstrahlung (below with the subscript ') also contributes to the intensity. Generally speaking, the bremsstrahlung can ige in comparison with an amorphous medium, under channeling conditions. No oretical analysis of this problem is available. Nevertheless, to give an idea of the

Table 1

Parameters of the potential for the ⟨111⟩ axis and some characteristics of the radiation

al	u_1 (10^{-10} m) $T = 293$ K	V_0 (eV)	U_0 (eV)	β	a_s (10^{-10} m)	$c = \frac{L_{rad}}{L_{ph}}$	R	ω_{ch} (MeV)	L_0 (mm)
(d)	0.040	29	103	0.025	0.326	0.61	1.87	21.1	15.6
i	0.075	54	106	0.150	0.30	0.57	0.80	23.3	15.3
/	0.082	135	280	0.135	0.306	0.49	1.16	37.0	4.8
r	0.061	165	358	0.122	0.272	0.48	1.64	47.0	3.6
e	0.068	180	363	0.145	0.276	0.48	1.46	46.6	3.15
e	0.085	91	191	0.13	0.30	0.51	0.53	31.1	4.3
93 K)	0.050	417	937	0.115	0.215	0.50	1.48	96.2	0.65
K)	0.030	348	1255	0.027	0.228	0.50	2.38	105.0	0.61

plitude of thermal vibrations, V_0, β, a_s parameters of the potential (6), U_0 depth of the potell, c ratio of the radiation length to the effective length of photon absorption, $R = I_{as}/I_{br}$ ratio = 1 GeV, ω_{ch} frequency calculated by means of (16) at $\varepsilon_0 = 1$ GeV, L_0 optimal thickness of rystal at $\varepsilon_0 = 1$ GeV.

nitude of the effect, we shall make use of the model of a corresponding amorphous ium for a description of the bremsstrahlung. Assuming the condition (4) to be fied, for the bremsstrahlung intensity at depth l we find

$$\frac{dI_{br}}{d\Omega} = \frac{I_{br}}{\pi g(l)} \equiv \frac{1}{\pi g(l)}\,\frac{\varepsilon}{L_{rad}}\,. \tag{9}$$

[1, 2] the energy variation will be taken into account in an adiabatic approximawith due regard for both mechanisms of radiation losses. Hence, for the energy epth l we have

$$\frac{\varepsilon(s)}{\varepsilon_0} = \frac{e^{-s}}{1 + R(\varepsilon_0)\,(1 - e^{-s})} = G(s)\,, \tag{10}$$

or $s = l/L_{rad}$, ε_0 is the initial energy and $R(\varepsilon) = I_{as}/I_{br}$. Substituting $\varepsilon(s)$ into nd (9), we find

$$\frac{dI_{ch}}{d\Omega} = \frac{\alpha}{(2\pi)^2}\,\frac{\varepsilon_0^3 R(\varepsilon_0)}{m^2 L_{rad}}\,G^2(s)\,f(s)\,,$$
$$\frac{dI_{br}}{d\Omega} = \frac{\alpha}{(2\pi)^2}\,\frac{\varepsilon_0^3}{m^2 L_{rad}}\,G(s)\,f(s)\,, \tag{11}$$

e

$$f(s) = \left[\frac{1}{2}\,(1 + R)^2\,(e^{2s} - 1) - 2R(1 + R)\,(e^s - 1) + R^2 s + \frac{l_d}{L_{rad}}\right]^{-1}. \tag{12}$$

$R \equiv R(\varepsilon_0)$, l_d is defined in (3), and $G(s)$ is given by (10).

given by eq.(2) with a corresponding expression obtained in CFA BKS(1987) for the uniform distribution over transverse coordinates. So eq.(2) reproduces the energy dependence of coherent contribution to the radiation length $L_{ch} = \varepsilon/I_{ch}(\varepsilon)$ inherent to CFA which as mentioned above is valid in a wide energy range. For the sake of possible use, we have fitted our results for the function $r(\varepsilon)$ in the energy interval $\varepsilon < 5GeV$ by a polynomial

$$r(\varepsilon) = \sum_{n=0}^{9} a_n \varepsilon^n ,$$

where ε is measured in GeV and coefficients a_n for $<110>$-axis of Si and Ge crystals and for $<111>$-axis of W crystal are calculated. The fitting provides the accuracy better than 1 percent for Si and Ge and better than 3 percent for W.

The position of a maximum in the spectrum given by eq.(2) is always consistent with the estimate (1). For relatively small energies when $\rho_c \ll 1$ and correspondingly $u_0 \ll 1$, we can neglect the first term in the right-hand side of eq.(3) since $\rho_c/\chi_s = 2ma_s \gg 1$. In this case the spectrum (2) has a maximum at $\omega = \omega_{max} \simeq 0.05\varepsilon u_0 \simeq 2\varepsilon\sqrt{\rho_c}/(ma_s)$ which evidently coincides in this (dipole) approximation with eq.(1). When $\rho_c \gg 1$ and CFA is valid the spectrum (2) reproduces not only the position of a maximum but also the shape of spectral distributions like those shown in Fig.2 of BKS(1987) ob-

where a_s is the screening radius of a corresponding potential and

$$\rho \simeq (2V_0/m\theta_0)^2 \; for \; \theta_0 > \theta_c$$

and

$$\rho \simeq \rho_c = 2V_0\varepsilon/m^2 \; for \; \theta_0 < \theta_c .$$

The estimate BKS(1987) for the characteristic frequency of emitted photons ω at given frequency of motion ω_0 reads

$$u \equiv \frac{\omega}{\varepsilon - \omega} \simeq \frac{2N\omega_0\varepsilon}{m^2(1+\rho/2)}, \qquad (1)$$

where N is the characteristic number of emitted harmonics. Note that $N = 1$ for $\rho \leq 1$ and $N \propto \rho^{3/2}$ for $\rho \gg 1$. Using also that $\omega_0 \sim \theta_0/a_s$, we suggest to describe the radiation from channeled and moving not very high above the potential barrier particles the following heuristic intensity spectrum:

$$\frac{dI_{ch}}{d\omega} = \frac{r(\varepsilon)\varepsilon}{u_0(\varepsilon)}\left[1 + \frac{1}{(1+u)^2}\right]\left(\frac{u}{u_0}\right)^{1/3} \ln\left(\frac{u_0}{u}\right)\vartheta(u_0 - u), \qquad (2)$$

where $\vartheta(z) = 1$ for $z > 0$ and $\vartheta(z) = 0$ for $z < 0$,

$$u_0 = \frac{25}{6}\chi_s + 80\frac{1}{ma_s}\frac{\sqrt{\rho_c}}{(2+\rho_c)}. \qquad (3)$$

The function $r(\varepsilon)$ in eq.(2) is determined by the condition of the coincidence of the total intensity

$$I_{ch}(\varepsilon) = \int_0^{\varepsilon} d\omega \left(\frac{dI_{ch}}{d\omega}\right)$$

and modifications of incoherent contributions are small, distinctions in the soft cascade development in crystal and amorphous media are mainly due to the coherent contribution to the radiation. This contribution changes the shape of photon spectra, enriching their soft part and noticeably diminishing the effective radiation length L_{ef} determined by the relation

$$L_{ef}^{-1} = \tilde{L}_{rad}^{-1} + L_{ch}^{-1} .$$

So, for the $< 111 >$ axis of tungsten, we find $L_{ef} \simeq 0.13\,cm$ at $\varepsilon = 2GeV$ and $L_{ef} \simeq 0.08\,cm$ at $\varepsilon = 5GeV$, which are several times less than the amorphous value $L_{rad} \simeq 0.35\,cm$. Thus in a crystal the initial electron is converted into photons along appreciably shorter length than in a corresponding amorphous medium, while further development of the soft shower in both media is more or less the same. Hence the most pronounced distinctions of shower characteristics in the amorphous and crystal case appear for small thicknesses. It is clear that for the valuable use of crystal properties in the case of suggested target composed of crystal and amorphous layers, the former must be of a few L_{ef} thick.

tained within the approximation mentioned . We have compared the shape of the spectrum (2) with available experimental data, but this procedure is somewhat indirect for several reasons. Sometimes very thin samples were used where the distribution of electrons over transverse coordinates was far from being uniform, sometimes energy loss spectra were measured which are noticeably different from true intensity spectra, sometimes emitted photons were collimated that also results in a change of the observed shape of spectra. Nevertheless, a qualitative agreement of the spectrum (2) with known experimental data holds for all energies beginning with $900\,MeV$.

The contribution to any process going on in a crystal is a sum $Y = Y_{coh} + Y_{inc}$ where, generally speaking, the incoherent contribution Y_{inc} differs from the amorphous value Y_{am}. The scale of this modification depends on the process under consideration. For the total intensity of the incoherent radiation and the quantity $\tilde{L}_{rad} = \varepsilon / I_{br}$ connected to it, the typical scale of diminishing of I_{br} as compared to I_{am} at room temperature is depending on media 9 to 13 per cent. The diminishing of the total probability of pair-production is of the same order of magnitude. In particular, we obtain for tungsten in the case of a full screening $\tilde{L}_{rad} = 1.1\,L_{rad}$. As far as the coherent contribution to the pair-production probability is negligible in the considered energy region

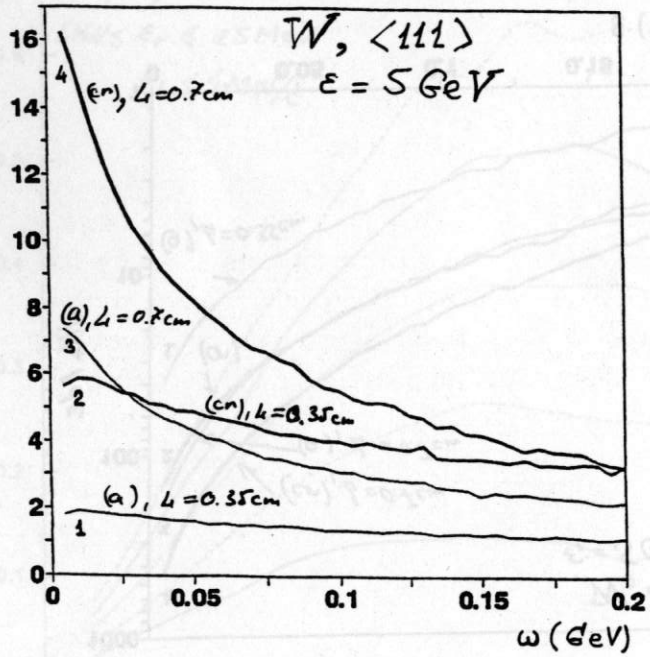
W, <111>
ε = 5 GeV
(cr), L=0.7cm
(a), L=0.7cm
(cr), L=0.35cm
(a), L=0.35cm
ω (GeV)

Fig. 1 (b)

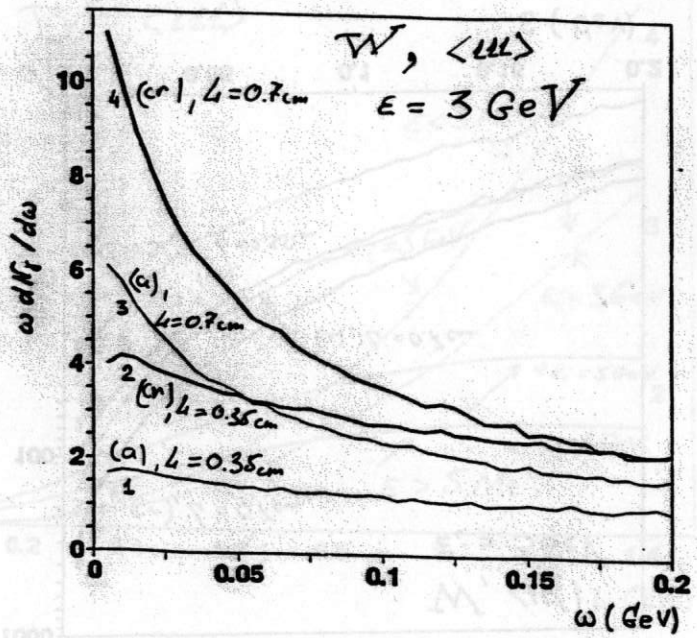
W, <111>
ε = 3 GeV
(cr), L=0.7cm
(a), L=0.7cm
(cr), L=0.35cm
(a), L=0.35cm
ω dN_γ/dω
ω (GeV)

Fig. 1(a)

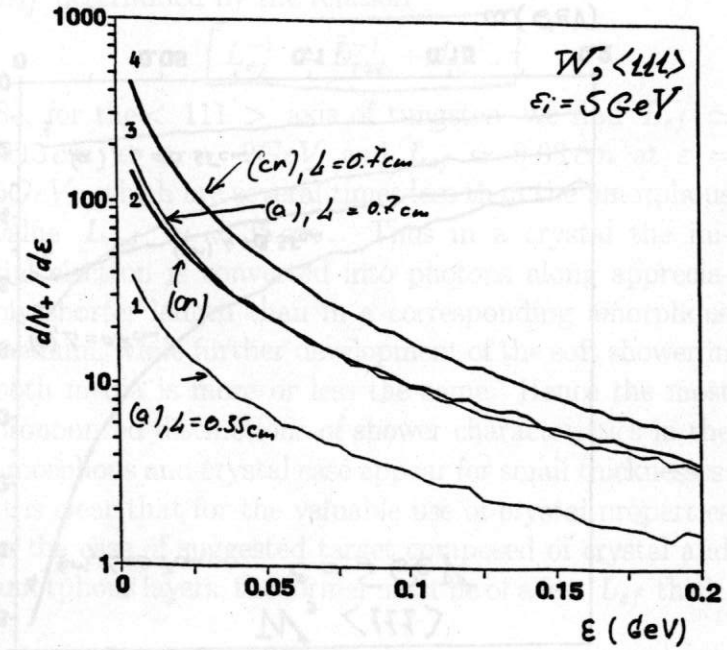
W, <111>
ε_i = 5 GeV
(cr), L = 0.7 cm
(a), L = 0.7 cm
(cr)
(a), L = 0.35 cm
$\varepsilon dN_+/d\varepsilon$
ε (GeV)
1000
100
10
1
0
0.05
0.1
0.15
0.2
1
2
3
4

Fig. 2 (b)

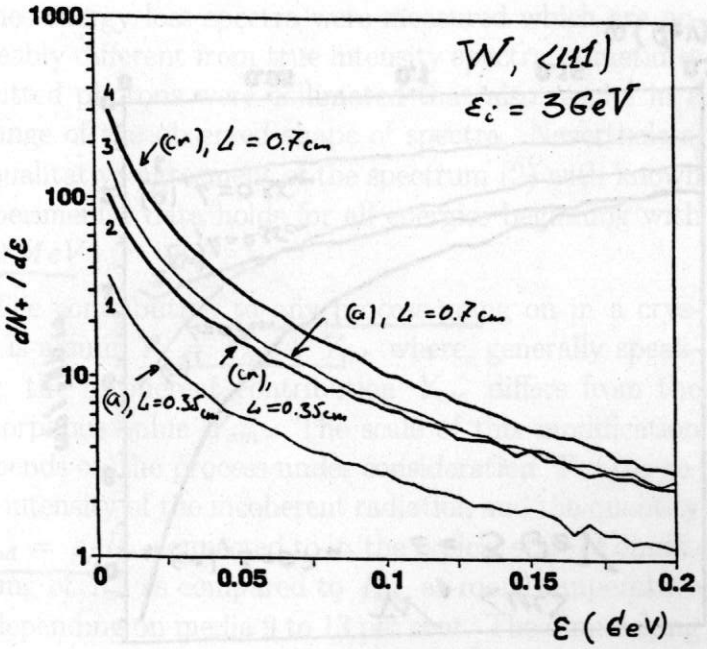
W, <111>
ε_i = 3 GeV
(cr), L = 0.7 cm
(a), L = 0.7 cm
(cr), L = 0.35 cm
(a), L = 0.35 cm
$dN_+/d\varepsilon$
ε (GeV)
1000
100
10
1
0
0.05
0.1
0.15
0.2
1
2
3
4

Fig. 2 (a)

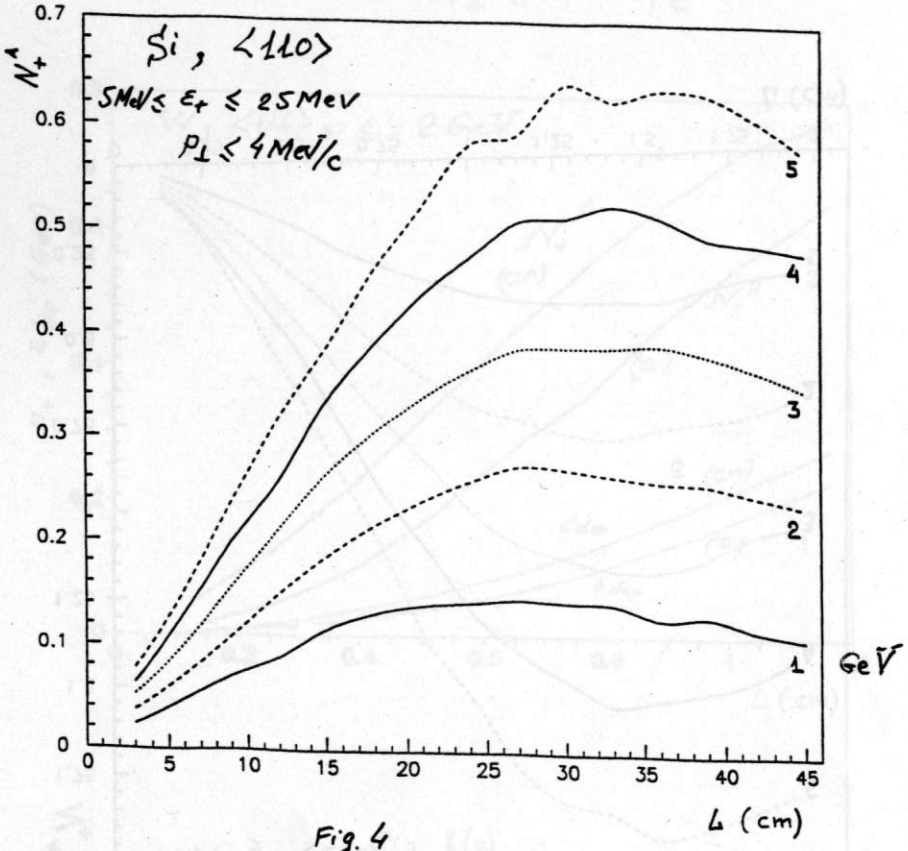
Si , <110>
5MeV ≤ ε+ ≤ 25MeV
P⊥ ≤ 4MeV/c
N+
0.7
0.6
0.5
0.4
0.3
0.2
0.1
0
0 5 10 15 20 25 30 35 40 45
L (cm)
5
4
3
2
1
GeV

Fig. 4

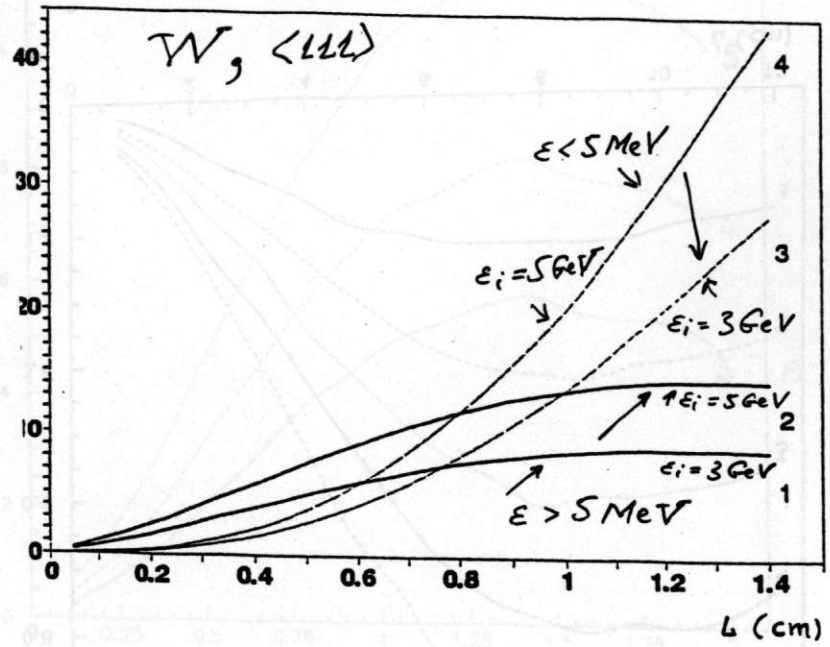
W, <111>
ε < 5MeV
εi = 5GeV
εi = 3GeV
εi = 5GeV
εi = 3GeV
ε > 5MeV
40
30
20
10
0
0 0.2 0.4 0.6 0.8 1 1.2 1.4
L (cm)
4
3
2
1

Fig. 3

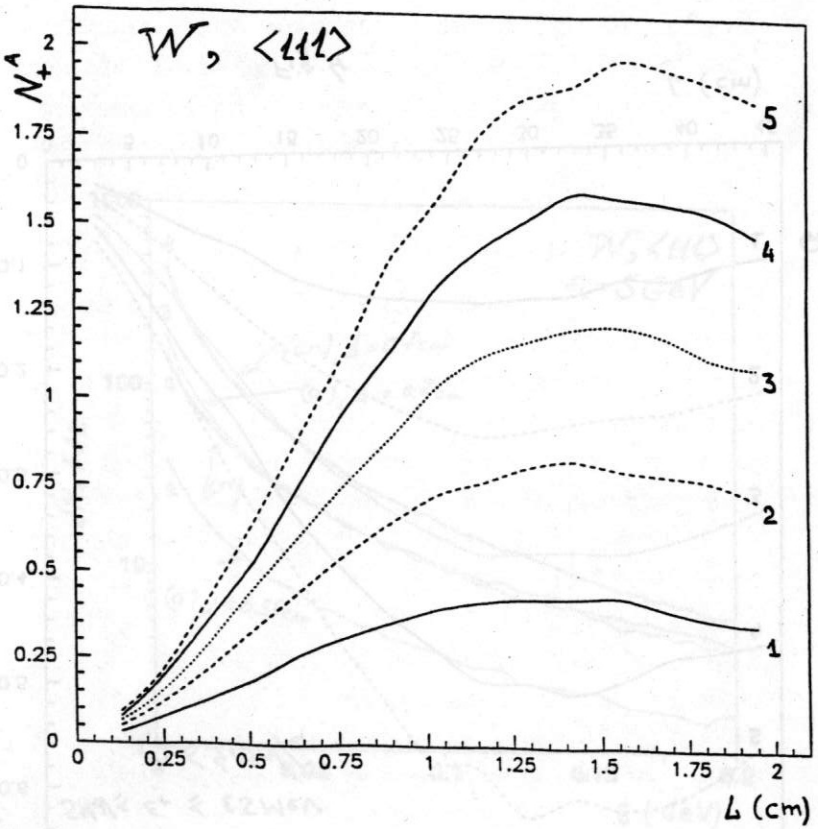
W, <111>
N_+^2
1.75
1.5
1.25
1
0.75
0.5
0.25
0
0.25
0.5
0.75
1
1.25
1.5
1.75
2
L (cm)
5
4
3
2
1

Fig. 6

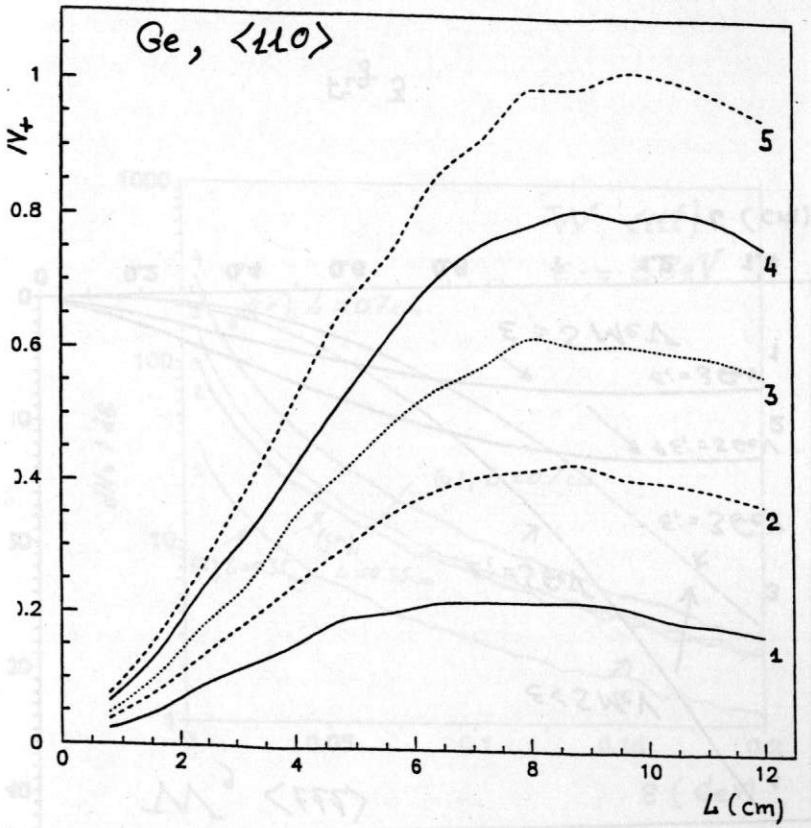
Ge, <110>
N_+
1
0.8
0.6
0.4
0.2
0
2
4
6
8
10
12
L (cm)
5
4
3
2
1

Fig. 5

A : accepted $5\,MeV \leq \varepsilon_+ \leq 25\,MeV$

$p_\perp \leq 4\,MeV/c$

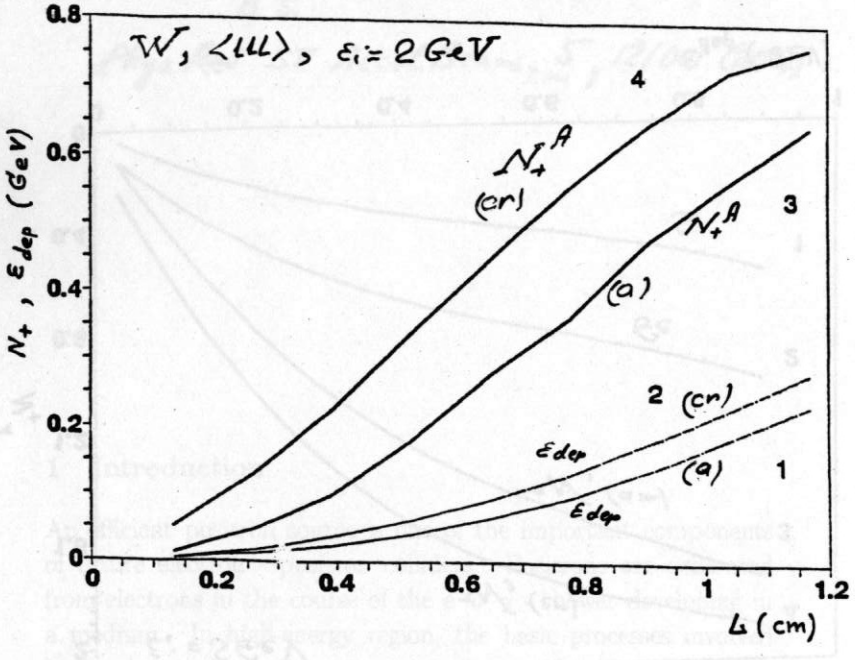

Fig. 8 (a)

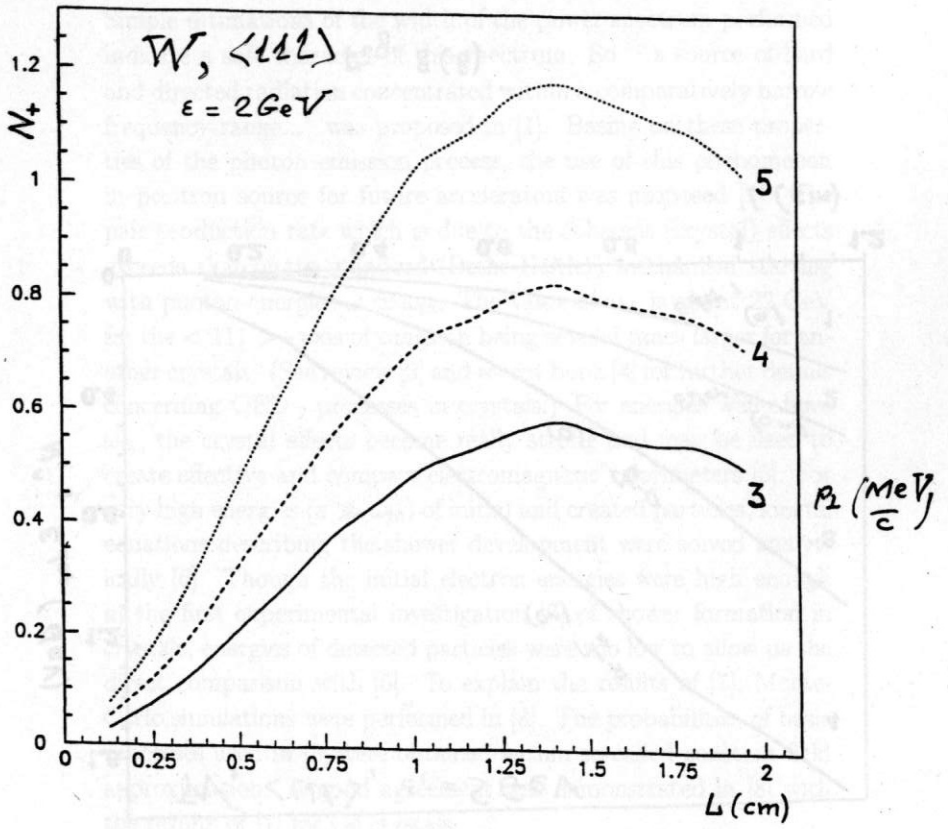

Fig. 7

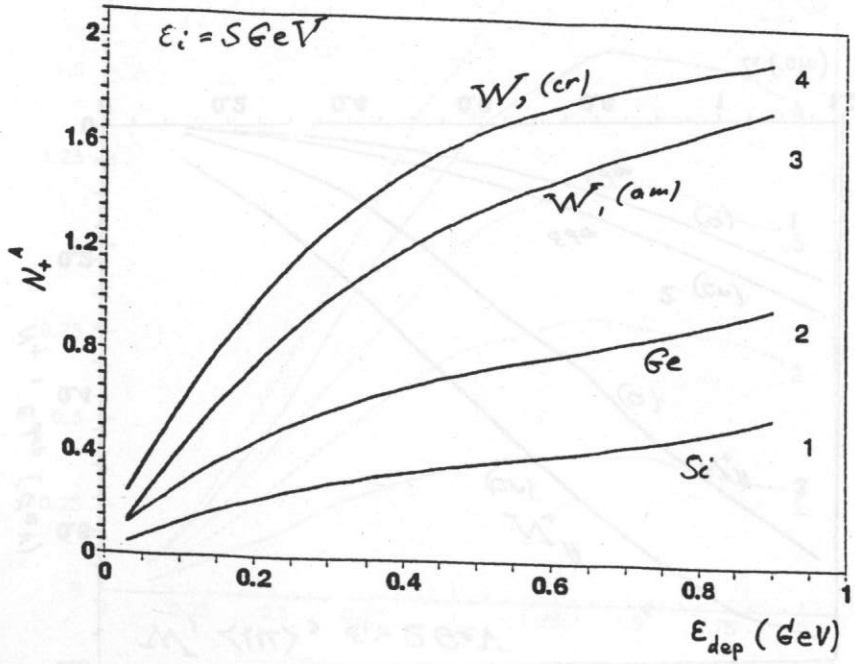
$\varepsilon_i = 5$ GeV
W, (cr)
W, (am)
Ge
Si
4
3
2
1
N_+^A
ε_{dep} (GeV)
0
0.4
0.8
1.2
1.6
2
0.2
0.4
0.6
0.8
1

Fig. 9

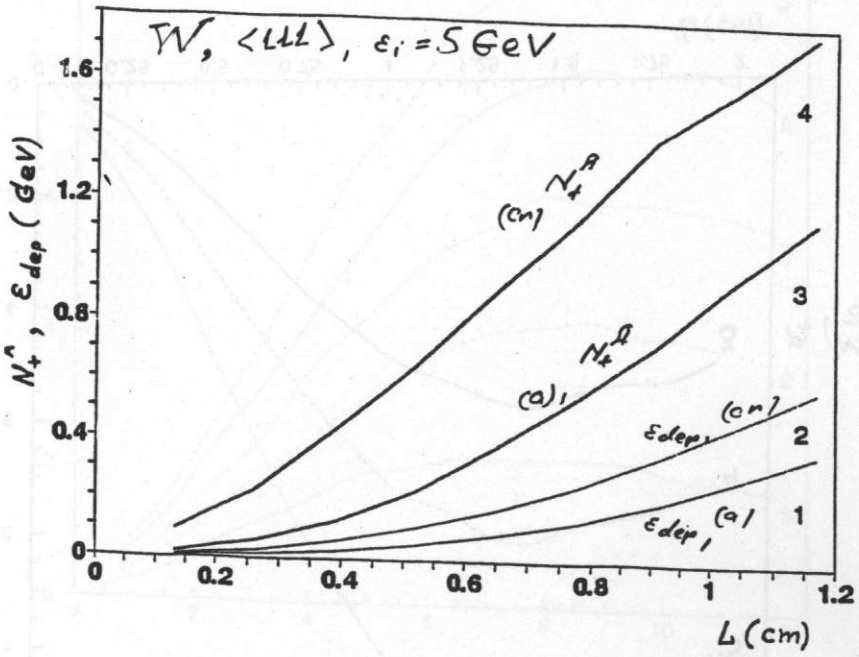
W, $\langle 111 \rangle$, $\varepsilon_i = 5$ GeV
N_+^A (cr)
N_+^A (a),
ε_{dep}, (cr)
ε_{dep}, (a)
4
3
2
1
N_+^A, ε_{dep} (GeV)
L (cm)
0
0.4
0.8
1.2
1.6
0.2
0.4
0.6
0.8
1
1.2

Fig. 8 (B)

Comparison of theory with experiment for positron production from high-energy electrons moving along crystal axes

B. S.
Phys. Rev ST Accel. Beams, 5, 121001 (2002)
V. N. Baier, V. M. Strakhovenko

1 Introduction

An efficient positron source is one of the important components of future electron - positron colliders. Positrons are generated from electrons in the course of the $e^-e^+\gamma$ - shower developing in a medium. In high-energy region, the basic processes involved in the shower development are typically considerably enhanced in oriented crystals as compared with corresponding amorphous media . The most pronounced effects take place at axial alignment when initial electrons are moving along the main axes of a crystal. This alignment alone will be considered below. According to [1],the radiation intensity in a crystal exceeds that of the conventional bremsstrahlung starting with electron energies $\varepsilon \sim 1$ GeV. Simple estimations of the width of the power spectrum performed indicate a soft character of this spectrum. So '...a source of hard and directed radiation concentrated within a comparatively narrow frequency range...' was proposed in [1]. Basing on these properties of the photon emission process, the use of this phenomenon in positron source for future accelerators was proposed [2]. The pair production rate which is due to the coherent (crystal) effects exceeds that of the standard (Bethe-Heitler) mechanism starting with photon energies $\omega \simeq \omega_{th}$. The value of ω_{th} is about 22 GeV for the $< 111 >$ - axis of tungsten being several times larger for another crystals. (See review [3] and recent book [4] for further details concerning QED - processes in crystals.) For energies well above ω_{th}, the crystal effects become really strong and may be used to create effective and compact electromagnetic calorimeters [5]. For very high energies ($\varepsilon \gg \omega_{th}$) of initial and created particles, kinetic equations describing the shower development were solved analytically [6]. Though the initial electron energies were high enough in the first experimental investigation [7] of shower formation in crystals, energies of detected particles were too low to allow us the direct comparison with [6]. To explain the results of [7], Monte-Carlo simulations were performed in [8]. The probabilities of basic processes used in [8] were obtained within so-called constant field approximation. A good agreement was demonstrated in [8] with the results of [7] for Ge crystals.

When the initial electron energy is below ω_{th}, photons are mainly emitted with energies $\omega \ll \omega_{th}$ and so, up to minor modifications (see [9], [10]), the pair production process proceeds in a crystal as in an amorphous medium. The enhancement of radiation from initial electrons is thereby the main crystal effect in this en-

present the scale, let us list some values ω_{max} where this spectrum is maximum: $\omega_{max}(1GeV) \simeq$31 MeV, $\omega_{max}(4GeV) \simeq$170 MeV, and $\omega_{max}(8GeV) \simeq$490 MeV. Note that the width of the spectrum is typically several times larger than ω_{max}. The increase in the number of relatively soft photons turns out to be much more pronounced than that in the total radiation intensity. In the end, just this fact leads to the substantial enhancement of the positron yield from crystal targets.

Recently the positron production in axially aligned single crystals was studied in two series of experiments performed at CERN [12], [13] and KEK [14], [15]. The initial energy of electrons was 3 GeV [14], 6 and 10 GeV [13], 8 GeV [15], and 10 GeV [12]. In all cases the initial electron beam was aligned with the $< 111 >$ - axis of the tungsten crystal that sometimes served as the crystal part of the hybrid target which contained an additional amorphous tungsten target. A noticeable enhancement of the low-energy positron yield was observed in all experiments cited above when the yield from the crystal target was compared with that from the amorphous target of the same thickness. The experimental results and our theoretical estimations presented in the next Section display a rather good agreement with each other.

2 Comparison of theory with experiment

Theoretical results for the conditions of the experiments cited above were obtained using the approach developed in [11] and [10] where various positron and photon distributions as well as deposited energies in different crystals were calculated for the energy range of initial electrons from 2 to 300 GeV. In these papers, all the formulas used in Monte-Carlo simulations of the specific $e^-e^+\gamma$ - shower characteristics are given in the explicit form. Remember that our ergy region. The substantial advance in the description of shower formation at axial alignment was caused by the invention of the semi - phenomenological radiation spectrum [11] . This allows one to consider the relatively low (of a few GeV) energy range of the initial electrons which is presumed for the efficient positron source. The radiation intensity increases with the initial electron energy. As a result, at some energy the effective radiation length L_{ef} in the crystal becomes smaller than the conventional radiation length L_{rad} and continues its decrease at further increase of the energy. All numerical examples will be given below for the electron beam aligned with the $< 111 >$ - axis of the tungsten crystals. Then we have for the quantity L_{ef} defined as in Sec.3 of [11]: L_{ef}(1 Gev) $\simeq$ 0.166 cm, L_{ef}(4 Gev) $\simeq$ 0.084 cm, and L_{ef}(8 Gev) $\simeq$ 0.061 cm. In the hybrid target which consists of the crystal part followed by the amorphous one, the thickness of the crystal constituent of several L_{ef} is obviously quite enough. Indeed, at the depth $L_0 \approx (3 \div 4)L_{ef}$ most of the particles, including the initial electrons, are sufficiently soft to reduce the coherent contribution to the radiation to the level of the incoherent one. Thereby, the further development of the shower proceeds more or less in the same way for the crystal or amorphous type of the remaining part of the target. We emphasize that the crystal part $L \leq L_0$ of the target serves as the radiator, and secondary charged particles are still not so numerous at this stage of the shower development. Therefore only a small portion of the total energy loss is deposited in the crystal part of the target which considerably reduces a danger of its overheating. The softness of photon spectra is another important feature of the crystal radiator giving additional advantages for the positron production in comparison with the entirely amorphous target. To get more definite idea concerning the shape of the power spectrum one can use its explicit form given by Eq.(2) in [11]. To

positrons having energies in the 5÷45 MeV range. We emphasize that the relative difference between measured and simulated results typically does not exceed 20 % in both spectral and angular distributions as seen in Fig.1. We are aware that preliminary results for another settings used in the same experiment do not contradict with the estimated scale of the difference between the data and theoretical predictions. We hope that this interrelation will not become worse after performing the complete analysis of the data which now is underway. This analysis will also give more detailed information concerning spectral - angular distributions of positrons depending on initial electron energies and target thicknesses.

2.2 Experiment (KEK) at $\varepsilon_0 = 3$ GeV

The main goal of the experiment [14] was an attempt to apply the crystal target to the working electron/positron linac, the injector for the electron - positron collider B - Factory at KEK. Thus, the acceptance conditions for created positrons were determined by the momentum acceptance of the positron linac with the matching section which is 8.2 MeV/c $< p <$ 11.6 MeV/c and $p_\perp <$ 2.4 MeV/c. The hybrid target used consists of 1.7 - mm - thick tungsten crystal followed by 7 - mm - thick amorphous tungsten. The observed positron yield was enhanced by the factor 1.40 when the $< 111 >$ crystal axis was aligned with 3 GeV incident electron beam as compared to the case of the disoriented crystal. Our number for this enhancement is 1.47 being only 5 % larger than the experimental one. Note that in the experiment [14] the crystal and amorphous parts of the hybrid target were separated by the distance of 70 mm. This circumstance, which, in principle, may slightly change the enhancement value, was not taken into account in our calculation. Recollect that the amount of the energy deposited in the crystal part (ε^{cr}_{dep}) of the hybrid target may be much smaller than that simplified description of the shower development takes into account coherent (induced by the regular motion of particles in the field of crystal axes) and incoherent (like that in an amorphous medium) mechanisms of photon emission and pair production processes. The multiple scattering and the ionization energy loss of electrons and positrons are taken into account neglecting crystal effects. The coherent radiation from channelling and moving not very high above the axis potential barrier particles is described using the semi - phenomenological spectrum suggested in [11]. The corresponding computer code was developed. This allows one to calculate energy, angular, and coordinate distributions of positrons emergent from the crystal or hybrid target and to find an amount of the energy deposition. We think that the investigation of such distributions should be the main object of the experiments having the creation of the crystal assisted positron source as their ultimate aim.

2.1 Experiment (CERN) at $\varepsilon_0 = 10$ GeV

Among experiments cited above, spectral - angular distributions of created positrons were measured only in WA103 experiment at CERN (see [12], [13]) where our code was used in simulations as the event generator. This simulation allowed for the acceptance conditions and the efficiency of the detectors used. Shown in Fig.1 taken from [13] is one example of the measured and simulated distributions of positrons from 10 - GeV electrons aligned with the $< 111 >$- axis of the 8 - mm - thick crystal tungsten.

The angular acceptance conditions in WA103 experiment were approximately $|\vartheta^{out}_V| \leq 1.5°$ for the vertical and $0 \leq \vartheta^{out}_H \leq 25°$ for the horizontal angle of outgoing positron with respect to the initial electron beam direction. We shell see below that the shape of the positron spectrum depends on the degree of collimation. The one-dimensional (over ϑ^{out}_H) angular distribution is presented for

$\vartheta_{out} \leq 24°$ are overlapping within precision better than 1 % starting from $\varepsilon_{cr}^{(1)} \simeq 55$ MeV. In turn, from $\varepsilon_{cr}^{(2)} \simeq 110$ MeV, the same happens with curves corresponding to $\vartheta_{out} \leq 24°$ and $\vartheta_{out} \leq 12°$. Such behavior is also seen in Fig.2 (b) for the amorphous target where $\varepsilon_{am}^{(1)} \simeq 50$ MeV and $\varepsilon_{am}^{(2)} \simeq 105$ MeV. In other words, positrons with energies $\varepsilon > \varepsilon^{(1)}$ are practically concentrated within the cone $\vartheta_{out} \leq 24°$ and those with $\varepsilon > \varepsilon^{(2)}$ have $\vartheta_{out} \leq 12°$. In accordance with this picture, the spectral maximum is shifted to the right while the width of the distribution increases when the collimation angle decreases. The enhancement μ, being bin-by-bin ratio of the positron yield from the crystal target to that from the amorphous one at the same collimation, is almost constant for $\varepsilon <$ 45 MeV and monotonically decreases with growing positron energy. This means that positron spectra from the crystal target are softer. Somewhat lower values of $\varepsilon^{(1)}, \varepsilon^{(2)}$ in the amorphous case point at the same feature. For given collimation, the variation of the enhancement is about 20 % over the whole energy interval presented in Fig.2. The maximum values of the enhancement at different collimation are $\mu_{max}(\vartheta_{out} \leq 180°) \simeq 6.09$, $\mu_{max}(\vartheta_{out} \leq 24°) \simeq 5.92$, $\mu_{max}(\vartheta_{out} \leq 12°) \simeq 5.67$, and $\mu_{max}(\vartheta_{out} \leq 1°) \simeq 5.29$. Apparently, they diminish as the collimation angle does so. Shown in Fig.3 is the same as in Fig.2 but for the target thickness $L =$ 9.0 mm. The yield at $\vartheta_{out} \leq 1°$ (open circles) is multiplied now by 30. The qualitative behavior of spectra depending on the collimation angle at $L = 9.0$ mm is the same as at $L = 2.2$ mm. However, all the spectra become softer for the larger target thickness. This is indicated already by the increase in $\varepsilon^{(1)}$, $\varepsilon^{(2)}$ values which are now $\varepsilon_{cr}^{(1)} \simeq 85$ MeV, $\varepsilon_{cr}^{(2)} \simeq 185$ MeV, $\varepsilon_{am}^{(1)} \simeq 75$ MeV, $\varepsilon_{am}^{(2)} \simeq 165$ MeV. It is clear that the magnitude of the yield from the thicker target is essentially larger but this increase is different in the crystal and amorphous cases. For example, in the energy range $\varepsilon < 45$ MeV

(ε_{dep}^{am}) in the amorphous one. Such interrelation of ε_{dep}^{cr} and ε_{dep}^{am} should take place in the case of [14], where the crystal thickness is about 1.8 L_{ef} (see discussion in the Introduction). This is confirmed by our calculations which give $\varepsilon_{dep}^{cr} \simeq 11$ MeV and $\varepsilon_{dep}^{am} \simeq$ 277 MeV per one incident electron.

2.3 Qualitative features of positron distributions and experiment (KEK) at $\varepsilon_0 = 8$ GeV

In [15] the positron production efficiency from 2.2 - mm, 5.3 - mm and 9.0 - mm - thick tungsten crystals was measured using an 8 - GeV electron beam. Positrons produced in the forward direction with momenta 10, 15 and 20 MeV/c were detected by the magnetic spectrometer. Thus, only several points in the energy distribution were determined under hard collimation conditions. Therefore, before going on to the comparison of the experimental results with our, let us remind some important qualitative features of spectral - angular distributions using 8 GeV electrons and the $< 111 >$ - axis of the tungsten crystals as an example. For the sake of comparison, the corresponding distributions for amorphous tungsten will be presented as well. Below all the quantities characterizing the positron yield are normalized per one incident electron.

The use of matching systems implies some collimation (typically $\vartheta_{out} \leq 25°$) of outgoing positrons. Shown in Fig.2 is the energy dependence (energy step is equal to 10 MeV) of the positron yield from crystal (a) and amorphous (b) targets of the same thickness $L = 2.2$ mm. In the case of the hard collimation, when $\vartheta_{out} \leq 1°$ (open circles), the yield is multiplied by 10 to make it visible. The larger the positron energy, the smaller is the typical value of ϑ_{out} since both production and multiple scattering processes are characterized by smaller angles for higher energies. This is seen in Fig.2 (a) where the spectral curves for $\vartheta_{out} < 180°$ and that for

at $L = 9.0$ mm. These factors turn out to be practically (within an accuracy of a few percent) independent of the total positron momentum p. This fact can be easily understood if we assume that the width of the angular distribution of positrons is completely due to multiple scattering being, thereby, proportional to p^{-1}. Such assumption is confirmed by results of the calculation shown in Fig.5 for two groups of positrons. One of them contains positrons having momentum in the interval $p \in (8.5 \div 11.5)$ Mev/c , for another group $p \in (17 \div 23)$ Mev/c.

For the given target, the width of the angular distribution of positrons with $p \approx 10$ Mev/c is approximately twice as much that for $p \approx 20$ Mev/c as expected. The width of every distribution evidently increases when we go on to the thicker target of the same kind. Comparing angular distributions from crystal and amorphous targets of the same thickness, we find that at $L = 9.0$ mm the distributions are somewhat (about 1.5°) wider in the crystal case for both groups. In units of FWHM of the distribution from the crystal target these differences are about 6.5 % at $p \approx 10$ Mev/c and 14 % at $p \approx 20$ Mev/c. At $L = 2.2$ mm the distribution from the crystal target is wider by 15.5 % at $p \approx 20$ Mev/c whereas this is narrower by 10 % at $p \approx 10$ Mev/c.

Going on to the comparison of our results with those obtained in [15], let us remind that to perform an accurate comparison of such kind, exact information is needed concerning the acceptance conditions and registration efficiency of detectors in the experiment. As noted in [15], at $p = 20$ Mev/c, the momentum acceptance ($\Delta p/p$) was 3 % (FWHM) and the polar angle acceptance was less than 20 mrad (FWHM). Since the shape of the acceptance curves was unavailable to us, we have tried to simulate experimental conditions using the same angular collimation $\vartheta_{out} \leq \vartheta_{out}^{max}$ and the same value of $\Delta p/p$ for all momenta and targets. So, at the calculation the yield is increased by $6 \div 7$ times for a crystal and by $17 \div 20$ times for amorphous samples. As a result, the enhancement at $L = 9.0$ mm is almost 3 times less than at $L = 2.2$ mm in this energy range. At $L = 9.0$ mm the enhancement is peaked in the first bin ($\varepsilon \in (5 \div 15)$ MeV) for every collimation. Its maximum values are $\mu_{max}(\vartheta_{out} \leq 180°) \simeq 2.25$, $\mu_{max}(\vartheta_{out} \leq 24°) \simeq 2.15$, $\mu_{max}(\vartheta_{out} \leq 12°) \simeq 2.08$, and $\mu_{max}(\vartheta_{out} \leq 1°) \simeq 2.06$. The enhancement monotonically decreases with growing positron energy and approximately halves at $\varepsilon \approx 250$ MeV. Thus, positron spectra from the crystal target are softer at $L = 9.0$ mm as well, and this property is much more pronounced in comparison with $L = 2.2$ mm.

Matching systems can be characterized also by the maximum transverse momentum $p_\perp^{max}$ of accepted positrons. In this connection, spectra of positrons having $p_\perp < p_\perp^{max}$ are of undoubted interest. Such spectra at $L = 2.2$ mm (a) and at $L = 9.0$ mm (b) from crystal and amorphous targets are shown in Fig.4. In contrast to the case of the pure angular selection (cf. Figs.2,3 the position of spectral maxima at limited $p_\perp$ values is always in the first bin ($\varepsilon \in (7.5 \div 12.5)$ MeV). Corresponding maximum values are $\mu_{max}(5\ MeV/c) \simeq 5.82$, $\mu_{max}(2.5\ MeV/c) \simeq 5.62$ at $L = 2.2$ mm and $\mu_{max}(5\ MeV/c) \simeq 2.17$, $\mu_{max}(2.5\ MeV/c) \simeq 2.11$ at $L = 9.0$ mm. The enhancement monotonically decreases with growing positron energy. Its variation over the whole energy interval presented in Fig.4 is about 15 % at $L = 2.2$ mm and 40 % at $L = 9.0$ mm. So, for this selection too, positron spectra from crystal targets are softer than those from amorphous targets of the same thickness. The interesting feature of spectral curves in Fig.4 is the similarity of those obtained for two different values of $p_\perp^{max}$ from the same target. The scaling factors η are $\eta_{cr} \simeq 2.6$, $\eta_{am} \simeq 2.5$ at $L = 2.2$ mm and $\eta_{cr} \simeq 3.1$, $\eta_{am} \simeq 3.0$

In contrast to the magnitude of the positron yield, the enhancement is not very sensitive to the acceptance conditions. The calculated values of the enhancement(theory) are presented in Table 1 along with those taken from Table 1 of [15] (experiment). Purely statistical errors are figured in Table 1 as theoretical ones. The relative error in PPE was estimated as $N_{ef}^{-1/2}$, where N_{ef} is the mean number of events in the phase space corresponding to the acceptance conditions used in calculations. The total statistics was chosen so that approximately to equalize values of N_{ef} for amorphous and crystal targets of the same thickness. At given total statistics, the quantity N_{ef} increases with growing positron momentum in accord with a shape of the positron spectra at hard collimation shown in Figs. 2,3. This fact leads to a better statistical accuracy for larger momentum. We emphasize that the differences of the estimated and experimental enhancement values are smaller than corresponding experimental errors for all momenta and samples figured in Table 1.

3 Conclusion

Using the simple computer code suggested in [11] and [10], we have compared the theoretical predictions for some characteristics of the electromagnetic shower developing in axially aligned crystals with experimental results reported in [12],[13] and [14],[15]. On the whole, theory and experiment are consistent within the experimental accuracy. From this comparison we also conclude that the accuracy provided by the existing simplified code is at least better than 20%. This accuracy may be slightly improved if we include into consideration some processes like annihilation of positrons or Compton scattering of photons which were ignored as corresponding cross sections are small in the energy region of interlation of the magnitudes of positron production efficiency (PPE), we simply put ϑ_{out}^{max} to 20 mrad. The value of $\Delta p/p$ was chosen to reproduce at applied collimation the experimental magnitude of PPE for the 9.0 - mm - thick amorphous target. Acting in this way, we have got $\Delta p/p = 3.2$ %. We realize that our regard for the acceptance conditions is rather rough. An additional inaccuracy was introduced when we determined the PPE numbers from Fig.5 of [15]. Note that the experimental numbers obtained in a such way, which are presented by filled symbols in Fig.6, do not reproduce exactly the whole set of mean experimental values for the enhancement given in Table 1 of [15]. Moreover, in Fig.5 of [15] there are no experimental points for 2.2 and 5.3 - mm - thick amorphous targets. For these two cases, we present in Fig.6 the values of PPE given by smooth - curve fits corresponding to simulation fitting in Fig.5 of [15]. Bearing all this in mind, we, nevertheless, can assert that a rather good agreement is seen in Fig.6 of the experimental results and our estimations. Relative difference of them is better than 13 % everywhere except the values of PPE at $p = 10$ and 15 Mev/c from both thinnest ($L = 2.2$ mm) targets, where the experimental yield is underestimated by 19 % to 42 %. Note that just for this thickness the largest inaccuracy was introduced while determining the PPE numbers from Fig.5 of [15] at $p = 10$ and 15 Mev/c, as the magnitude of the yield is especially small in this case.

Table 1: Enhancement of the positron yield from crystal targets

Momentum (MeV/c)	Enhancement (2.2-mm-thick)		Enhancement (5.3-mm-thick)		Enhancement (9.0-mm-thick)	
	theory	experiment	theory	experiment	theory	experiment
10	6.0 ± 0.5	6.5 ± 0.6	3.2 ± 0.3	3.4 ± 0.7	2.1 ± 0.2	2.3 ± 0.4
15	5.5 ± 0.3	6.2 ± 0.8	3.2 ± 0.2	3.2 ± 0.5	2.0 ± 0.1	2.0 ± 0.2
20	5.4 ± 0.2	5.1 ± 0.5	2.9 ± 0.1	3.0 ± 0.5	1.8 ± 0.1	1.8 ± 0.2

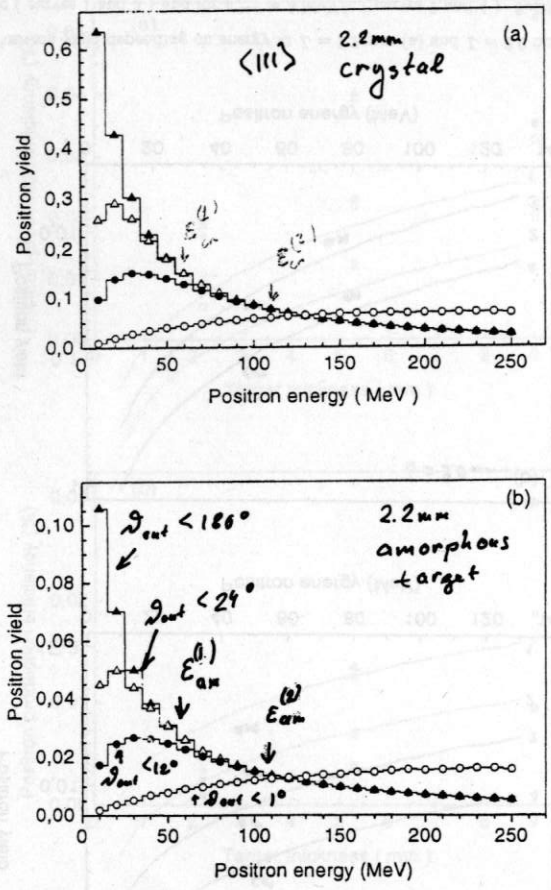

FIG. 2: Positron yield depending on energy from 2.2 - mm - thick crystal (a) and amorphous (b) targets at different collimation . Filled triangles - no collimation ($\vartheta_{out} \leq 180°$), open triangles - $\vartheta_{out} \leq 24°$, filled circles - $\vartheta_{out} \leq 12°$, and open circles - $\vartheta_{out} \leq 1°$ (multiplied by 10).

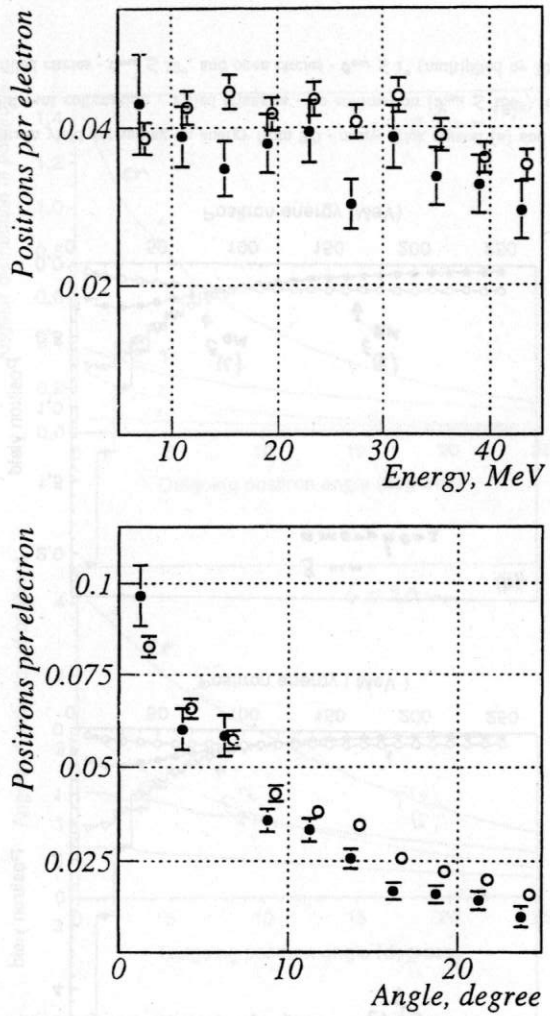

FIG. 1: Spectral (left) and angular (right) distributions of positrons from 10 GeV electrons traversing 8 - mm - thick crystal tungsten target along the < 111 >- axis. Open circles - simulation, filled circles - experiment.

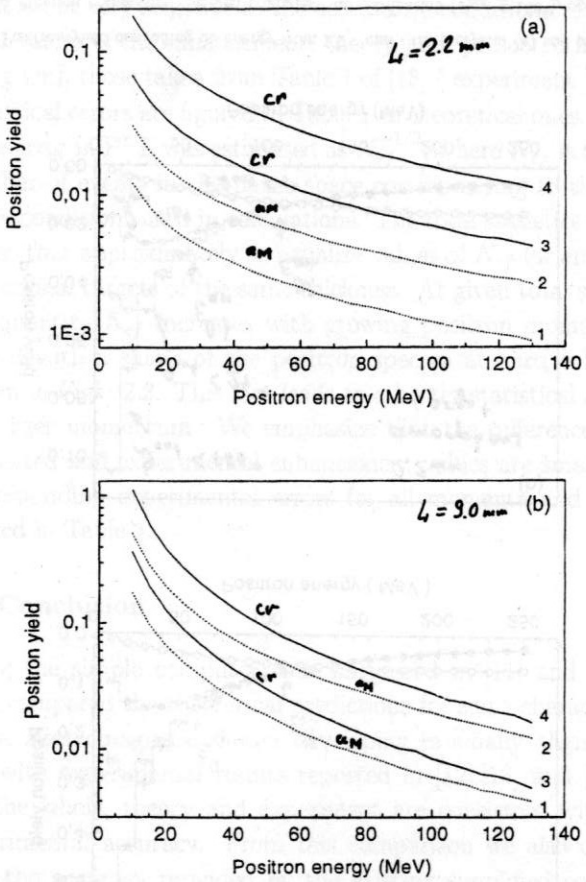

FIG. 4: Positron yield depending on energy at $L = 2.2$ mm (a) and $L = 9.0$ mm (b) for $p_{\perp}^{max} =$ 2.5 MeV/c (curves 1 and 3) and for $p_{\perp}^{max} = 5$ MeV/c (curves 2 and 4). Solid curves represent the yield from crystal and dotted from amorphous targets.

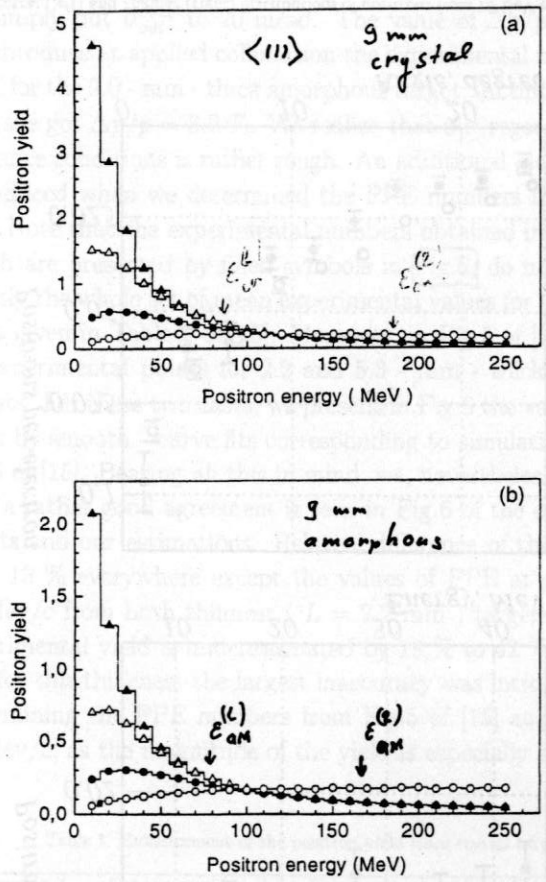

FIG. 3: Positron yield depending on energy from 9.0 - mm - thick crystal (a) and amorphous (b) targets at different collimation . Filled triangles - no collimation ($\vartheta_{out} \leq 180°$), open triangles - $\vartheta_{out} \leq 24°$, filled circles - $\vartheta_{out} \leq 12°$, and open circles - $\vartheta_{out} \leq 1°$ (multiplied by 30).

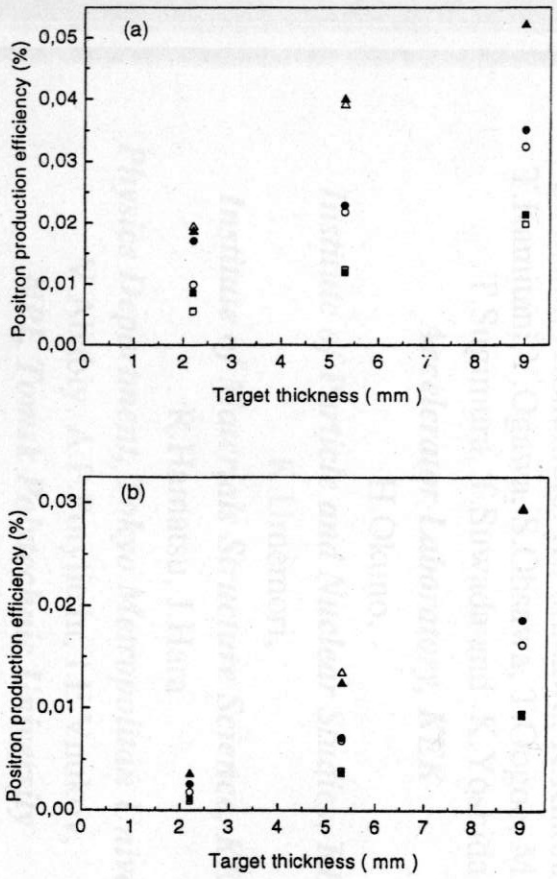

FIG. 6: Positron production efficiency from crystal (a) and amorphous (b) targets depending on thickness. Open symbols - our calculation, filled symbols - results from Fig.5 of [15]; △ are for $p = 20$ Mev/c, ○ are for $p = 15$ Mev/c, and □ are for $p = 10$ Mev/c.

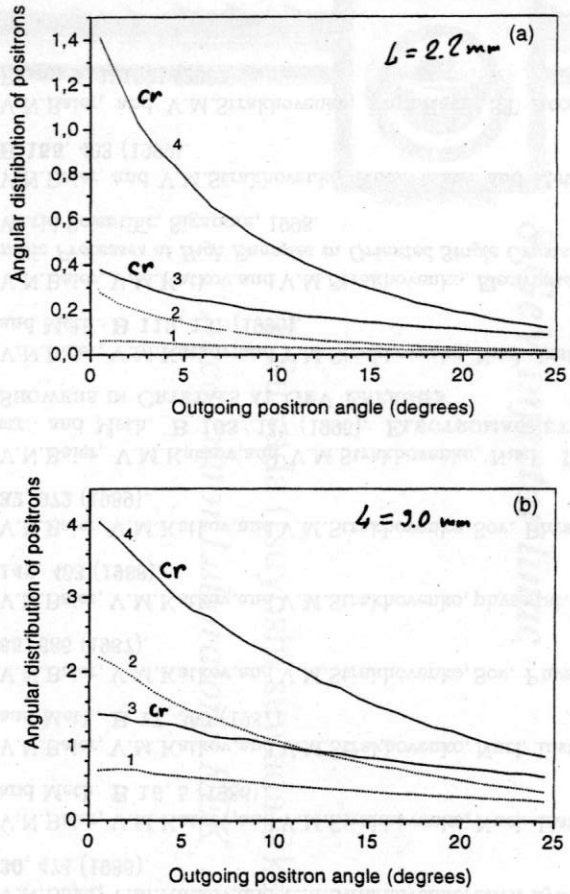

FIG. 5: Angular distribution $dN^{(+)}/d\Omega$ depending on outgoing positron angle at $L = 2.2$ mm (a) and at $L = 9.0$ mm (b) for $p_\perp \in (8.5 \div 11.5)$ Mev/c (curves 1 and 3) and for $p_\perp \in (17 \div 23)$ Mev/c (curves 2 and 4). Solid curves represent the yield from crystal and dotted from amorphous targets.

1. V.N.Baier, V.M.Katkov,and V.M.Strakhovenko, phys.stat.sol.(b) **133**, 583 (1986). RADIATION YIELD OF HIGH-ENERGY ELECTRONS IN THICK CRYSTAL
2. V.N.Baier, V.M.Katkov,and V.M.Strakhovenko, Sov.Phys.Dokl, **30**, 474 (1986).
3. V.N.Baier, V.M.Katkov,and V.M.Strakhovenko, Nucl. Instr. and Meth. **B 16**, 5 (1986).
4. V.N.Baier, V.M.Katkov,and V.M.Strakhovenko, Nucl. Instr. and Meth. **B 27**, 360 (1987).
5. V.N.Baier, V.M.Katkov,and V.M.Strakhovenko, Sov. Phys.JETP **65**, 686 (1987).
6. V.N.Baier, V.M.Katkov,and V.M.Strakhovenko, phys.stat.sol.(b) **149**, 403 (1988).
7. V.N.Baier, V.M.Katkov,and V.M.Strakhovenko, Sov. Phys.Usp. **32**, 972 (1989).
8. V.N.Baier, V.M.Katkov,and V.M.Strakhovenko, Nucl. Instr. and Meth. **B 103**, 147 (1995). ELECTROMAGNETIC SHOWERS IN CRYSTALS AT GEV ENERGIES
9. V.N.Baier, V.M.Katkov,and V.M.Strakhovenko, Nucl. Instr. and Meth. **B 119**, 131 (1996).
10. V.N.Baier, V.M.Katkov,and V.M.Strakhovenko, *Electromagnetic Processes at High Energies in Oriented Single Crystals*, World Scientific, Sigapore, 1998.
11. V.N.Baier, and V.M.Strakhovenko, Nucl. Instr. and Meth. **B 155**, 403 (1999).
12. V.N.Baier, and V.M.Strakhovenko, Phys.Rev. ST Accel. Beams **5**, 121001 (2002).